Petroleum Science 23 (2026) 157–177

Contents lists available at ScienceDirect

Petroleum Science

journal homepage: www.keaipublishing.com/en/journals/petroleum-science

Original Paper

Joint physics and model-guided pre-stack seismic inversion using double dual neural network

Jian Zhang [a,b], Hui Sun [a], Xing-Guo Huang [c,*], Li Han [c], Yan-Song Li [d]

[a] The Faculty of Geosciences and Engineering, Southwest Jiaotong University, Chengdu, 611756, Sichuan, China
[b] National Key Laboratory of Petroleum Resources and Engineering, China University of Petroleum (Beijing), Beijing, 102249, China
[c] College of Instrumentation and Electrical Engineering, Jilin University, Changchun, 130061, Jilin, China
[d] China MCC5 Group Corp., Ltd., Chengdu, 610063, Sichuan, China

ARTICLE INFO

Article history:
Received 28 February 2025
Received in revised form
13 July 2025
Accepted 4 September 2025
Available online 10 September 2025

Edited by Meng-Jiao Zhou

Keywords:
Pre-stack seismic inversion
Double dual neural network
Physics guided
Model guided

ABSTRACT

Pre-stack seismic inversion is used to calculate elastic parameters, including P-wave and S-wave velocities, as well as densities. These parameters play an integral role in the characterization of reservoirs, thereby enhancing the exploration and production process. Deep learning-based seismic inversion does not need a known physical system and can give satisfactory results with sufficient training data. The acquisition of such datasets for seismic inversion poses a significant challenge due to the exorbitant costs associated with drilling activities. Integrating domain knowledge, physical systems, and well log data into a deep learning-based seismic inversion framework is crucial for improving its efficiency and effectiveness. Nevertheless, existing data-driven approaches do not adequately exploit such information, thereby constraining their overall performance and applicability. Therefore, we develop a double dual neural network structure built upon the closed-loop neural network framework, which incorporates both physics and model information to mitigate the dependency on extensive labeled datasets. The information from the different domains is linked through a loss function, where one dual network is responsible for constraining the inversion results using physics information to ensure the physics consistency of the predictions, and the other dual network is responsible for constraining the inversion results using a priori model information to enhance the reliability of the predictions. The method makes full use of well-log data for network training when wells are available, as well as providing unsupervised learning and inversion under well-free conditions. The integration of qualitative and quantitative analyses proves instrumental in demonstrating the effectiveness of the proposed methodology through the use of synthetic and field pre-stack examples.

1. Introduction

Seismic inversion involves the transformation of seismic datasets into elastic and rock properties of geological formations in the subsurface, such as velocity, density, impedance, porosity, and fluid content. Pre-stack seismic inversion utilizes multi-angle gathers to provide an accurate image of the subsurface, and is an improvement on traditional post-stack inversion techniques (Shi et al., 2024b; Zhang et al., 2022a; Zhou et al., 2021). Physics-driven pre-stack seismic inversion methods have been the primary approach to this methodology for many years and have aided in the field of reservoir characterization. These techniques analyze seismic data collected from the surface and allow geophysicists to infer important subsurface parameters such as rock properties, density, and other elastic parameters. However, traditional physics-driven seismic inversion techniques have limitations. These techniques require the physical system (i.e., the mapping between seismic data and elastic parameters) to be known and often rely on the assumption of linear relationships between seismic reflections and rock properties (Grana et al., 2022; Wang et al., 2022b; Yu et al., 2024). The assumption of linearity can be problematic since the link between seismic data and elastic variables is not always straightforward. The subsurface is a complex

* Corresponding author.
E-mail address: xingguo.huang19@gmail.com (X.-G. Huang).
Peer review under the responsibility of China University of Petroleum (Beijing).

https://doi.org/10.1016/j.petsci.2025.09.008

and heterogeneous medium, and the mapping between seismic reflections and rock characteristics is nonlinear and highly variable. In such cases, physics-driven seismic inversion methods may not always produce accurate results due to uncertainties in the data and the assumptions made in the inversion process. To circumvent these limitations, researchers and practitioners are turning to data-driven seismic inversion approaches to avoid the pitfalls associated with restrictive assumptions (Arrowsmith et al., 2022; Lin et al., 2023; Mousavi and Beroza, 2022; Saikia et al., 2020; Yu and Ma, 2021). The deep learning (DL) approach has been applied in various industries and has been shown to uncover intricate patterns and relationships within large datasets, making it an ideal candidate for enhancing the precision of seismic inversion.

Data-driven seismic inversion is based on statistical theory and enables the transformation of seismic data into valuable insights regarding subsurface elastic properties. For many years, scholars and researchers have been trying various data-driven methods to solve the seismic inversion problem. Röth and Tarantola (1994) used a multilayered, partially connected neural network (i.e., fully-connected neural network, FCNN) to build links between synthetic seismic data and 1D velocities. The accuracy of the trained network reaches 80%, showing the ability of neural networks to solve complex nonlinear inverse problems. However, the vanishing gradient problem associated with the sigmoid activation function can lead to training difficulties in traditional FCNN architectures. Baddari et al. (2009) developed a radial basis function artificial neural network whose hidden layer is a Gaussian function, accomplishing impedance inversion and avoiding the vanishing gradient problem to some extent. Traditional FCNN inversion networks may overlook the spatial and temporal features present in seismic data due to the limitations of their architecture. Baddari et al. (2010) designed an Elman artificial neural network for performing seismic inversion, which allows them to handle temporal features within seismic data and deliver multi-step-ahead predictions. Feng et al. (2020) proposed a neural network model combined with a hidden Markov model, where the hidden Markov model explores spatial features in the seismograms, enabling accurate characterization of the spatial patterns of the rock characteristics and intrinsic depositional processes. However, while considering spatio-temporal information, the behaviour of a FCNN remains potentially free from control. Xu et al. (2019) constructed a physics-informed neural network based on a FCNN by introducing physical constraints to ensure that the inversion proceeding is properly steered. The above methods used one hidden layer, but they also demonstrated the effectiveness and advantages of data-driven methods for seismic inversion. With the massive developments of computer power over the last decade, neural networks containing many hidden layers (i.e., deep neural networks) are developed to extract richer features from the training data, thus further enhancing the reliability of inverted results.

Convolutional neural networks (CNNs) are being increasingly used in a variety of fields, such as medical image and speech identification, natural language processing, and driverless cars. A core strength of CNNs is their ability to extract spatial features from data, which makes them particularly suitable for tasks that involve analyzing images or time-series data with spatial information. Seismograms are records of ground motions characterized by strict horizontal and vertical spatial distribution, so CNNs have been extensively used in seismic surveys. Das et al. (2019) established an end-to-end matching of seismic records to impedance using a two-layer convolutional neural network, and subsequently performed impedance prediction using a network trained on synthetic data. Kazei et al. (2021) constructed an ensemble of CNNs to convert adjacent gathers to vertical 1D velocity model at the central location. Aleardi and Salusti (2021) proposed a pre-stack seismic inversion strategy combining a discrete cosine transform (DCT) re-parameterization with CNNs to achieve prediction of P- and S-wave velocity and density. Zhang et al. (2021, 2023) designed a hybrid neural network combining CNN and FCNN, and introduced the initial priori information to constrain the inverted results, which can alleviate the reliance on the training data, improve the network generalization ability, and ensures the stability of the inversion results. Sun et al. (2023) proposed a pseudo-well based CNN pre-stack seismic inversion, which constructs the training dataset required for deep learning using stochastic simulation methods, and subsequently performs synthetic model and field data testing and validation. Pan et al. (2024) constructed a CNN to predict subsurface rock fracture properties from pre-stack seismic azimuthal data. Furthermore, they employed an approximate Bayesian computation (ABC) method to estimate the posterior distribution of the predicted results, thereby quantifying the associated uncertainty. CNNs are primarily employed to extract spatial attributes from the input data, and in comparison recurrent neural networks (RNNs) have the advantage of extracting temporal attributes from the input data. Seismograms contains both spatial and temporal features, so a RNN can be employed for seismic inversion as well. Gao et al. (2021) used a long short-term memory (LSTM) network-based algorithm to model density prediction using seismic and well-log curves. Alzahrani and Shragge (2022) proposed a frequency-stepping velocity model construction method that builds a mapping of seismic data to velocities using a sequence-to-sequence RNN with built-in LSTM. Seismograms contains both spatio-temporal characteristics, so neither CNN or RNN alone are entirely applicable. The general approach is to design a network framework using both CNN and RNN functions, where CNN is used to extract spatial information while RNN is used to extract temporal information, and then the extracted spatio-temporal features are used to establish a mapping to the labels (Fabien-Ouellet and Sarkar, 2020; Guo et al., 2019; Wang et al., 2022a; Zhang et al., 2022b). These methods increase the generalization of the network to some extent, but they cannot eliminate the reliance on labeled data. They fall into the category of purely data-driven approaches, and their prediction lacks clear physical meaning.

Alternatively, physics-guided methods introduce physical laws into deep learning-based seismic inversion, alleviate the data independence of data-driven approaches, and boost the precision of inverted results. Biswas et al. (2019) combined CNNs and wave propagation law to predict elastic parameters, avoiding the need for labeled data for network training. Wang et al. (2021) proposed a physics-guided deep learning based seismic impedance inversion algorithm, while introducing bilateral filtering to improve the prediction accuracy and spatial continuity of the inversion results. Wang et al. (2022c) proposed a Cycle-GAN model to extract features from both unlabeled and labeled data for seismic impedance prediction. Zou et al. (2023) used a semi-unsupervised domain adversarial and spatial fusion inversion strategy to predict seismic impedance. Shi et al. (2024a) utilized closed-loop mapping to build a semi-supervised learning architecture to accomplish the inversion of seismic impedance, which alleviates the network's dependence on labeled data to some extent. Chen et al. (2024) developed a semi-supervised training loss function that combines deterministic forward operators with sampling operators, enabling simultaneous optimization of weights in both the forward and pseudo-inverse operators. Li et al. (2024) proposed a novel deep learning-based seismic inversion methodology that combines Bayesian techniques with physics-informed neural networks, enabling robust prediction of inversion results and

mitigating the requirement for extensive training datasets. Sun et al. (2024) established a physics-guided deep mixture density network to perform physics-informed probabilistic seismic inversion. Zhang et al. (2024) developed knowledge-embedded close-looped deep-learning framework, which alleviates the dependency on labeled data to a certain extent and reduces the uncertainty in inversion results. The inversion process based on deep learning still suffers from strong non-uniqueness when only physical laws are considered. In this case, it is useful to incorporate priori knowledge (e.g., priori initial models from the model domain) into the deep learning framework. Both in physics-driven and data-driven seismic inversion, it has been confirmed that incorporating priori information from the model domain improves inversion results (Bosch et al., 2010; Buland and Omre, 2003; Liu et al., 2023; Mousavi and Beroza, 2022). However, integrating this information to constrain seismic inversion results has always been difficult. Other research areas, such as image super-resolution processing and lake temperature modelling, have attempted to augment the capabilities of deep learning-based methods by exploiting constraints such as the laws of physics and priori knowledge of the model domain (Daw et al., 2022; Guo et al., 2020).

In this paper, we develop a double-dual network structure based on the physics-guided framework. This approach integrates both the physical and model domain information to alleviate the relying on training data for deep learning-based seismic inversion methods. When well-log data is available, well-log information from the data domain can be integrated into the network training process using traditional data-driven methods. One of the dual networks is responsible for using the physical laws to constrain the inversion results and ensure the physical validity of the predictions. It's worth noting that we utilize the forward network instead of the physical law formulation to both improve the physical constraints while speeding up the inverse network training process. The other dual network is responsible for using the priori information (i.e., initial model) from the model domain to constrain the inverted results and enhance the stability of the predictions. Inspired by image super-resolution processing (Chen et al., 2023; Zhu et al., 2023), we design an alternative constraint to narrow the possible space so that the predicted elastic parameters can rebuild the initial model. By imposing this constraint, we can approximate the underlying down-sampling kernel, thus narrowing the space of possible functions and finding the optimal solution. Ultimately, the two dual networks are coupled by a loss function to ensure the physical validity and robustness of the prediction results, and to realize the training and inversion applications of labeled/unlabeled data. Both the seismic records and the elastic parameters are a spatio-temporal data due to depositional and propagation effects. Consequently, spatio-temporal neural networks (STNNs), which consist of CNN and RNN, are utilized for both forward and inversion modeling. In this paper, we specifically implemented the framework using a spatio-temporal neural network as the sub-network within the double dual structure. However, other types of neural networks—such as CNNs, residual networks (ResNets), or others—could also be employed as sub-networks within the same double dual framework without altering its fundamental architecture.

The organization of this paper is as follows: we first describe the general framework of the deep learning-based seismic inversion and physics-guided deep learning-based seismic inversion. Next, we report in detail the specific structure and realization of the proposed double-dual network. Then, we present the experimental results of synthetic and field data as an example of the pre-stack seismic data, and compare the results with those of traditional methods. The last section provides some discussions and conclusions.

2. Methods

In this section, we first review purely data-driven and physically guided deep learning based seismic inversion methods (Wang et al., 2021; Zhang et al., 2021). Then, the proposed double-dual network structure and loss function are provided in detail. Finally, the specific architecture of the forward and inverse networks is provided to reproduce the experimental results.

2.1. Review of purely data-driven DL based seismic inversion

A purely data-driven DL based seismic inversion involves the use of labeled data pairs to train neural network (NN) models $f_{\mathrm{NN}}:\mathbf{d}\rightarrow\mathbf{m}$, where $\mathbf{d}$ denotes seismic data, $\mathbf{m}$ denotes elastic properties including velocity and density. After training the network using labeled data, it can be used to complete the prediction of elastic parameters for un-labeled seismic data. This framework, known as supervised learning seismic inversion, requires large amounts of training data to assure the effectiveness of the trained network. The initial stage in preparing the constructed neural network for seismic inversion involves training the network by formulating the loss function, using the following equation:

$$\mathcal{L}(m,\tilde{m})=\frac{1}{n}\arg_{\theta}\min\sum_{i=1}^{n}\left(m_i-\tilde{m}_i\right)^2 \tag{1}$$

where θ denotes the parameters of f_{NN} to be trained. n denotes the number of data sampling points. m and $\tilde{m}$ denote labeled data and network prediction results, respectively. The process of minimizing the error between predicted values and labeled data is a critical step in achieving an accurate network model. The trained network, representing the culmination of these iterations, is the outcome when specific conditions, such as reaching a set number of iterations or attaining a minimum error threshold, are satisfied. However, using only seismograms as network input leads to problems with network training and weak generalization (Zhang et al., 2021). To achieve better performance and robust of neural network models, it is useful to integrate priori knowledge of the model domain (i.e., low-frequency information about the parameters) into the training phase. This can be achieved through the implementation of a specific loss function that accounts for the initial model during training, as following:

$$\mathcal{L}_{\mathrm{MGNN}}(\theta)=\frac{1}{n}\left|\left|\mathbf{m}-f_{\theta}([\mathbf{d},\mathbf{m}_0])\right|\right|_2^2 \tag{2}$$

where $\mathbf{m}_0$ denotes initial elastic parameters model built from seismic horizon guided well-log interpolation. MGNN stands for model-guided neural network, i.e., a purely data-driven deep learning based seismic inversion method that takes model domain information (i.e., initial elastic parameters) along with seismic data as network input simultaneously.

2.2. Review of physically guided deep learning based seismic inversion

Pure data-driven DL based seismic inversion methods achieves good prediction when the training dataset is sufficient. However, labeled sets (i.e., well-log curves) are usually limited due to expensive drilling costs. In addition, the purely data-driven approach ignores the laws of physics, leading to predictions that

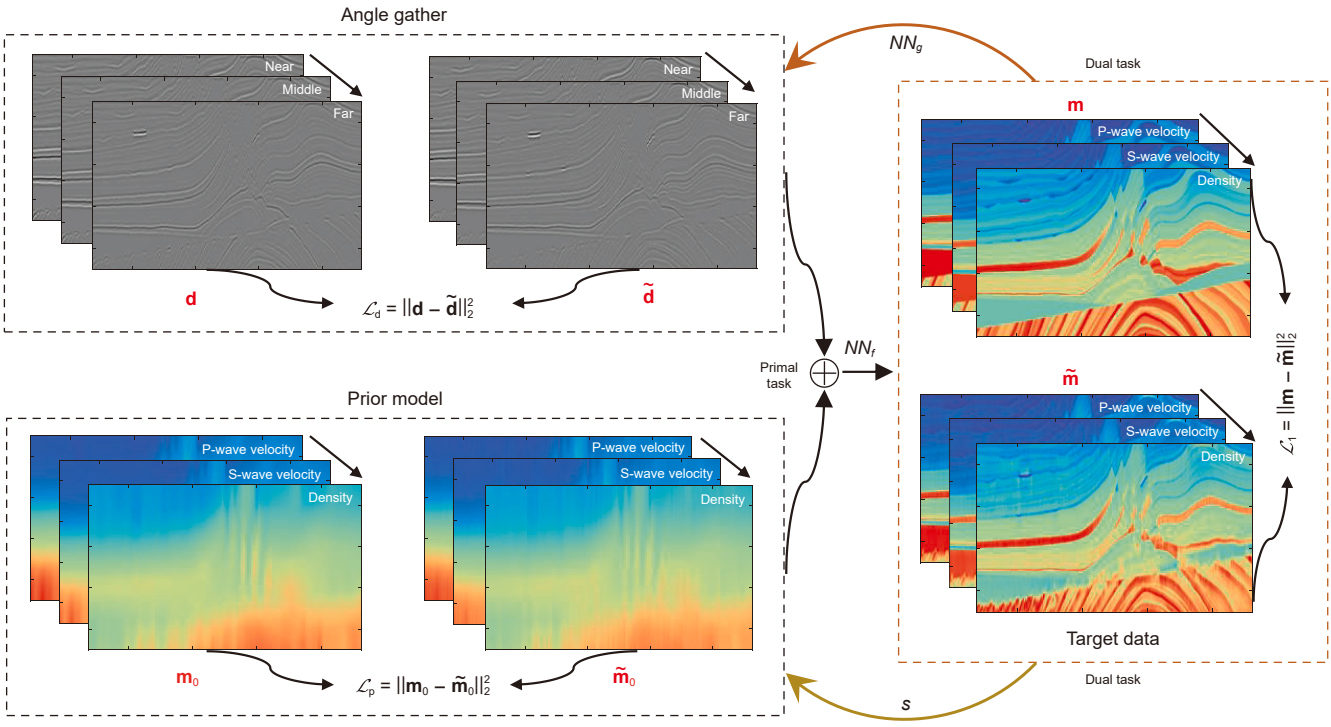

Fig. 1. The workflow of joint physics and model-guided deep learning-based seismic inversion. NN_g, NN_f, s represent forward neural network, inversion neural network and smooth filter operator, respectively.

may be inconsistent with known physical systems, i.e., the seismic records obtained using the predictions differ significantly from the actual seismic records acquired. To ensure that the predictions satisfy the known laws of physics while reducing the demand for massive labeled datasets in data-driven approaches, we can introduce physics-guided loss functions as follows:

$$\mathcal{L}_{\mathrm{PGNN}}(\theta,\vartheta) = \underbrace{||\mathbf{m} - f_\theta([\mathbf{d},\mathbf{m}_0])||_2^2}_{\mathcal{L}_1} + \underbrace{\lambda\cdot||\mathbf{d} - g_\vartheta(f_\theta([\mathbf{d},\mathbf{m}_0]))||_2^2}_{\mathcal{L}_2} \tag{3}$$

where θ is the parameters of the inverse network (f) to be trained, ϑ is the parameters of the forward network (g) to be trained. $\mathcal{L}_1$ is the labeled data loss function term, which plays an important role in integrating well-log data into the inversion network training process. $\mathcal{L}_2$ is the seismic data loss function term, which allows for the incorporation of known physical laws into the inversion network training process and enables training with labeled/unlabeled data. Note that g in the seismic data loss term can be either in the form of a network or a mathematical expression representing the forward process. In this paper, we construct training dataset based on the Zoeppritz equations (Eq. (4)) to train a network model. The trained network can build a mapping from elastic parameters to seismic data, thus replacing the laws of physics. λ is the weight parameter that controls the contribution of labeled data loss and seismic data loss. PGNN stands for physics-guided neural network, i.e., a seismic inversion method that incorporates priori knowledge of the

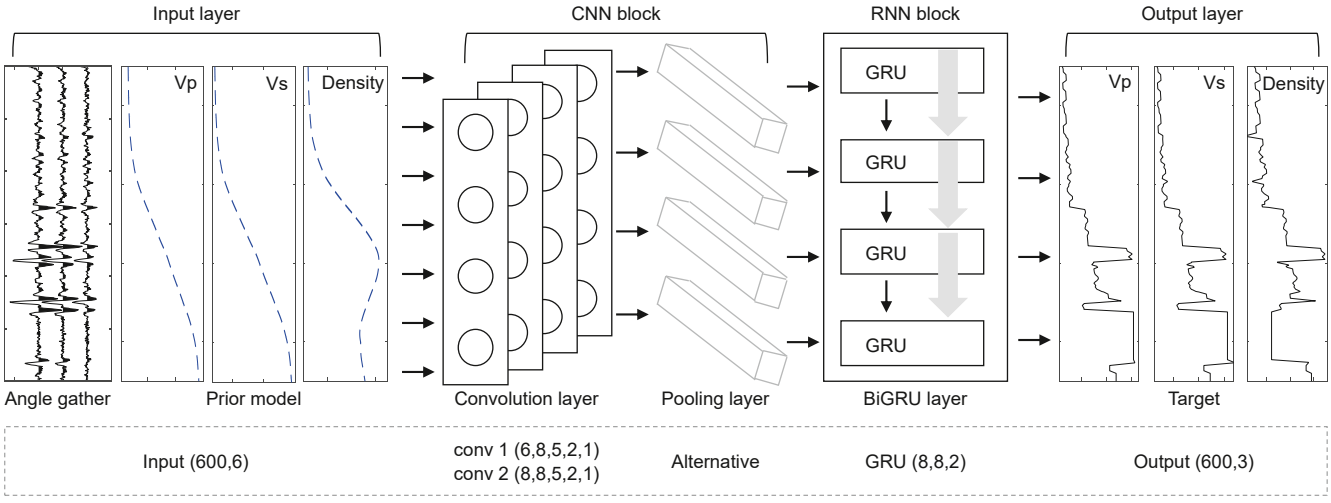

Fig. 2. Schematic of the adopted spatio-temporal neural network for pre-stack seismic inversion.

underlying physical laws into the training process of data-driven approach. By imposing constraints based on known physics principles, these methods can guide the learning process towards solutions that are physically feasible.

$$\begin{bmatrix} R_{pp} \\ R_{ps} \\ T_{pp} \\ T_{ps} \end{bmatrix} = \begin{bmatrix} -\sin\theta_1 & -\cos\varphi_1 & \sin\theta_2 & -\cos\varphi_2 \\ \cos\theta_1 & -\sin\varphi_1 & \cos\theta_2 & \sin\varphi_2 \\ \sin 2\theta_1 & \frac{v_{p1}}{v_{s1}}\cos 2\varphi_1 & \frac{\rho_2 v_{s2}^2 v_{p1}}{\rho_1 v_{s1}^2 v_{p2}}\sin 2\theta_2 & -\frac{\rho_2 v_{s2} v_{p1}}{\rho_1 v_{s1}^2}\cos 2\varphi_2 \\ -\cos 2\varphi_1 & \frac{v_{s1}}{v_{p1}}\sin 2\varphi_1 & \frac{\rho_2 v_{p2}}{\rho_1 v_{p1}}\cos 2\varphi_2 & \frac{\rho_2 v_{s2}}{\rho_1 v_{p1}}\sin 2\varphi_2 \end{bmatrix}^{-1} \begin{bmatrix} \sin\theta_1 \\ \cos\theta_1 \\ \sin 2\theta_1 \\ \cos 2\varphi_1 \end{bmatrix} \tag{4}$$

where R and T are reflection and transmission coefficients, respectively. $\cdot_{pp}$ stands for P-wave incident, P-wave reflected (or transmitted), and $\cdot_{ps}$ stands for P-wave incident, S-wave reflected (or transmitted). θ_1, θ_2 represent the angle of incidence and transmission of P-wave, respectively. φ_1, φ_2 represent the angle of incidence and transmission of S-wave, respectively. $v_{p1}, v_{p2}, v_{s1}, v_{s2}$, ρ_1, ρ_2 represent the P-/S-wave velocity, and density on both sides of the interface. The calculated reflection coefficients are convolved with given wavelets to obtain the corresponding seismic records.

Seismic inversion is an ill-posed problem since there are numerous elastic parameter models that can produce identical seismic records. Existing physics-guided DL based seismic inversion methods usually only consider well-log data and seismic data. It does not fully utilize the priori information from the model domain and is restricted by limited training dataset, leading to increased non-uniqueness in predictions away from well locations.

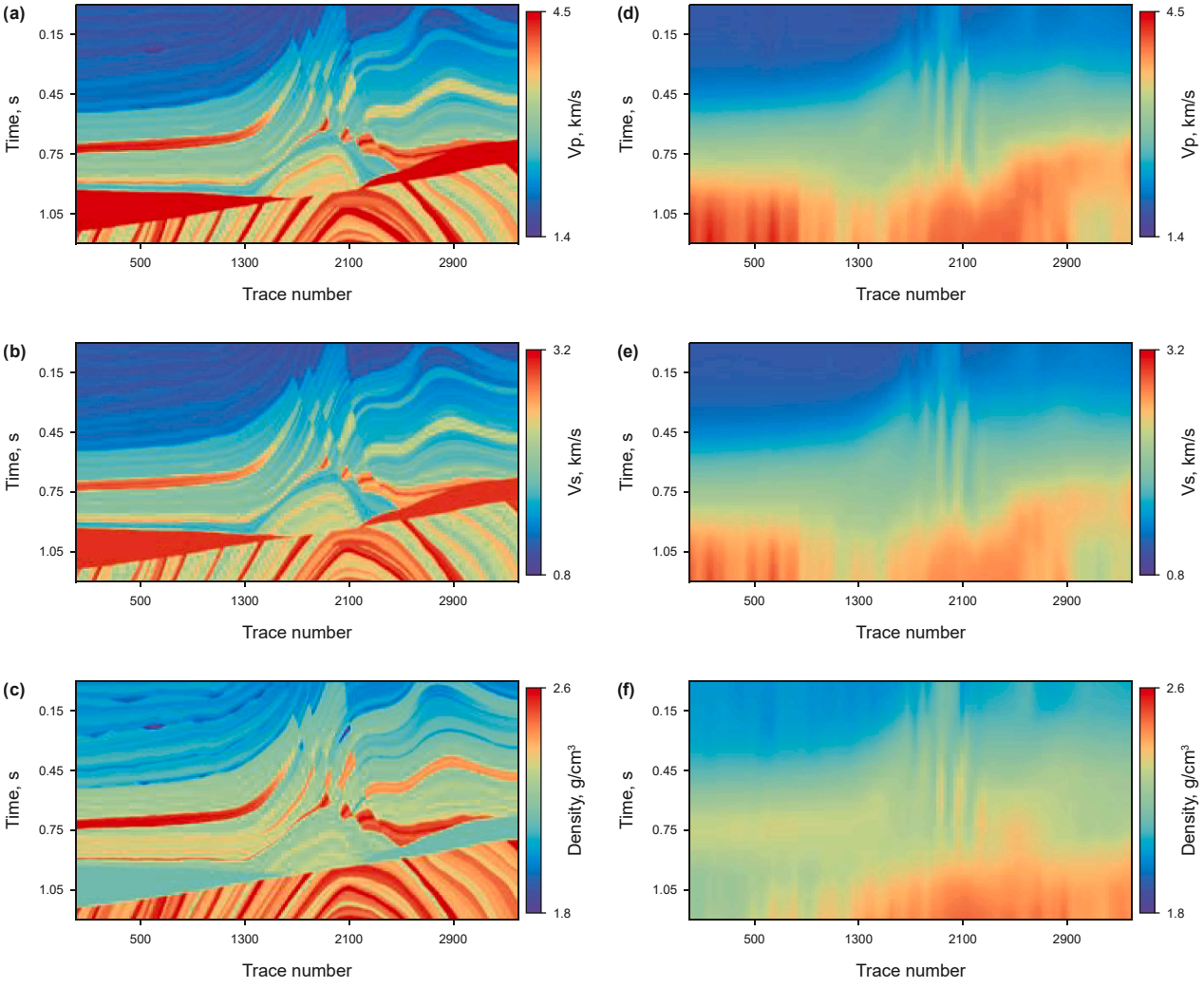

Fig. 3. Synthetic data test of Marmousi models: The reference values of **(a)** P-wave velocity (Vp), **(b)** S-wave velocity (Vs), and **(c)** density. The initial values of **(d)** Vp, **(e)** Vs, and **(f)** density.

2.3. Joint physics and model-guided deep learning based seismic inversion

A neural network model needs a large enough training dataset to accurately learn the patterns and relationships in the data. However, in some cases, there may be a lack of training dataset available for seismic inversion. When this occurs, the space of possible matching functions is very large, which makes training difficult. To overcome this problem, on the basis of PGNN, we present a double-dual regression proposal by integrating an auxiliary constraint with priori information from model domain (i.e., initial model).

Fig. 1 shows the workflow of joint physics and model-guided DL-based seismic inversion. The seismic data $\mathbf{d}$ and the low-frequency initial elastic properties (i.e., velocity and density) model $\mathbf{m}_0$ are used as inputs to complete the prediction of the target elastic parameter $\tilde{\mathbf{m}}$ via the primal task. In this paper, we use only three angle stacks (i.e., near-, middle-, and far-angle gathers) as inputs; in fact, more angle stacks are allowed. Subsequently, the predictions are manipulated by the dual task so that the predictions satisfy the given constraints (i.e., physics laws and priori knowledge). The primal and dual learning tasks constitute two closed-loop providing informational supervision for the training of the inversion network parameters. The concept of the dual closed-loop network is inspired by PGNN and super-resolution image processing techniques (Biswas et al., 2019; Guo et al., 2020). If the predictions $\tilde{\mathbf{m}}$ are the same as the true values m, then the seismic record $\tilde{\mathbf{d}}$ and low-frequency elastic parameter model $\tilde{\mathbf{m}}_0$ obtained by the dual tasks processing of $\tilde{\mathbf{m}}$ should be very close to the reference seismic record $\mathbf{d}$ and low-frequency elastic parameter model $\mathbf{m}_0$. With these two constraints, both the physical validity of the prediction results is guaranteed, and the space of functions that may be mapped is reduced, making it easier to learn better mappings to predict the elastic parameters.

If labeled data is available, we can further integrate it into the network training process. To enable the network to function effectively, we need to design an appropriate loss function. The labeled data loss ($\mathcal{L}_\mathrm{l}$), seismic data loss ($\mathcal{L}_\mathrm{d}$), and initial model loss ($\mathcal{L}_\mathrm{p}$) can be written as

$$\begin{cases} \mathcal{L}_\mathrm{l}(\theta) = \underbrace{\left|\left|\mathbf{m} - f_\theta([\mathbf{d}, \mathbf{m}_0])\right|\right|_2^2}_{\mathcal{L}_1} \\ \mathcal{L}_\mathrm{d}(\theta, \vartheta) = \underbrace{\left|\left|\mathbf{d} - g_\vartheta(f_\theta([\mathbf{d}, \mathbf{m}_0]))\right|\right|_2^2}_{\mathcal{L}_2} \\ \mathcal{L}_\mathrm{p}(\theta) = \underbrace{\left|\left|\mathbf{m}_0 - s(f_\theta([\mathbf{d}, \mathbf{m}_0]))\right|\right|_2^2}_{\mathcal{L}_3} \end{cases} \tag{5}$$

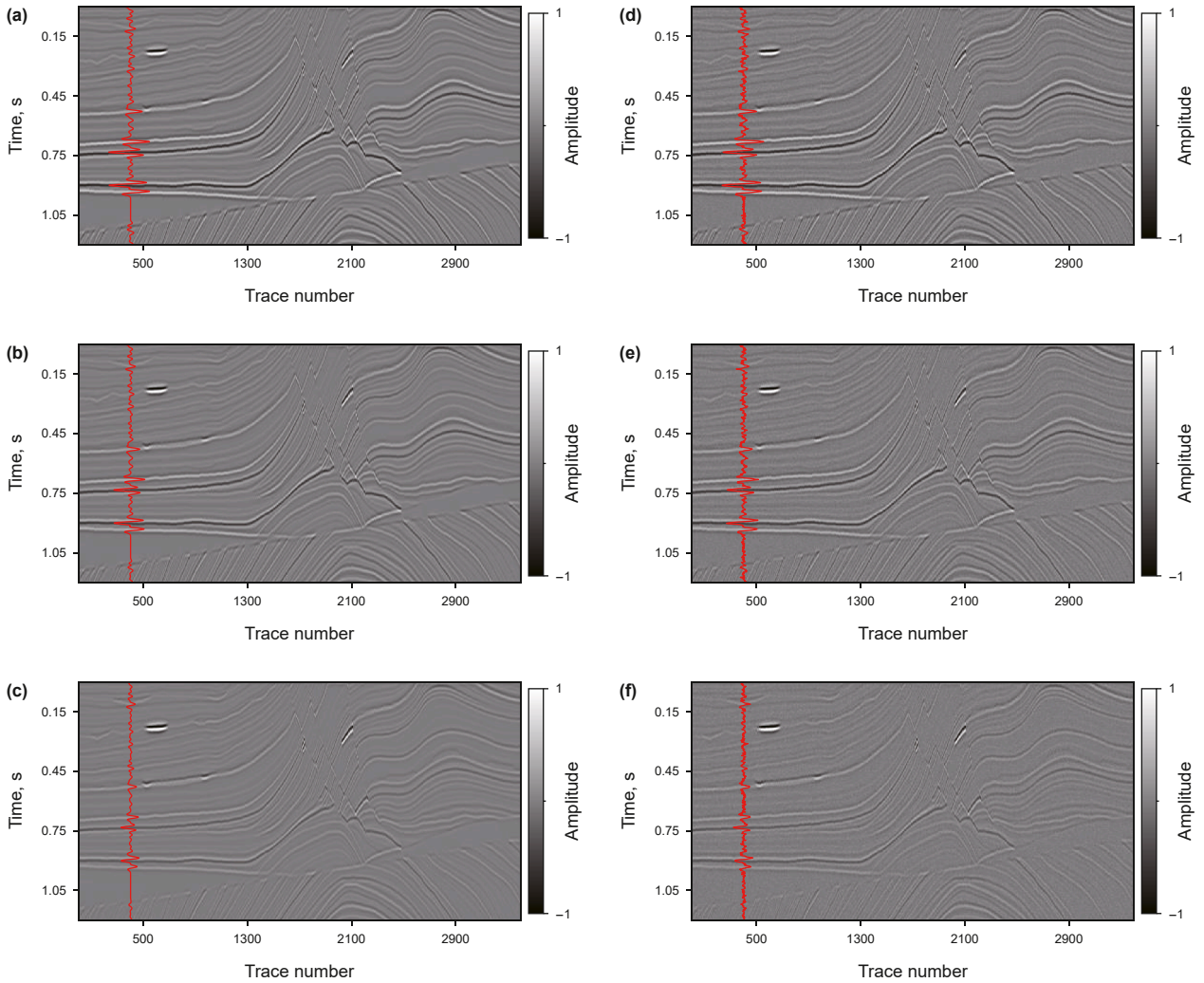

Fig. 4. The partial angle stacks from the Marmousi model. Noise-free: **(a)**–**(c)** near-, middle-, and far-angle gathers. Noisy (SNR = 5): **(d)**–**(f)** near-, middle-, and far-angle gathers.

where s denotes the filtering operator such that the prediction $s(\tilde{\mathbf{m}})$ is similar to the given initial model $\mathbf{m}_0$. In our experiments, we use an arithmetic mean filter to obtain the $\tilde{\mathbf{m}}$ to $\tilde{\mathbf{m}}_0$ mapping. It is notable that the optimal number of smoothing points will vary from task to task, which needs to be chosen on a task-specific in order to better match $\tilde{\mathbf{m}}_0$ and $\mathbf{m}_0$. θ stands for the parameters of the inversion network (f) to be trained, ϑ stands for the parameters of the forward network (g) to be trained. The strategy for training forward neural network g here is the same as the process of training the forward neural network in PGNN.

By learning these three tasks together, we create a joint physics and model-guided deep learning-based seismic inversion network. The training loss can be written as

$$\mathcal{L}_{\mathrm{PMGNN}}(\theta,\vartheta)=\lambda_1\mathcal{L}_1(\theta)+\lambda_2\mathcal{L}_2(\theta,\vartheta)+\lambda_3\mathcal{L}_3(\theta) \tag{6}$$

where λ_1, λ_2, λ_3 denote weight parameters that control the contribution of different losses to the training process. Relatively optimal weight parameters are determined through an iterative trial-and-error process in subsequent experiments. $\mathcal{L}_1$ contains only labeled data, but both labeled and unlabeled datasets can be included in $\mathcal{L}_2$ and $\mathcal{L}_3$. PMGNN stands for joint physics and model-guided neural network, i.e., a seismic inversion method that introduces physics laws and priori information from the model domain into a data-driven approach. Only the inversion network parameters θ are updated during the network training phase, while the parameters ϑ of the forward network are fixed. The specific training pseudo-code is reported in Algorithm 1.

Algorithm 1
Training procedure of the proposed PMGNN

Input: Labeled data: $\mathbf{m}^*$, $\mathbf{m}_0^*$, $\mathbf{d}^*$;
Unlabeled data: $\mathbf{m}_0$, $\mathbf{d}$;
Batch size for unlabeled data: n;
Set the values of λ_1, λ_2, λ_3
Load the pre-trained model g;
While *not convergent* **do**:
  Sample unlabeled data $\{m_{0i}, d_i\}_{i=1}^{n}$ from $\mathbf{m}_0$, $\mathbf{d}$;
  // Update f using labeled and sampled unlabeled data
  Update θ of f by minimizing the objective:
    $\lambda_1\mathcal{L}_1+\lambda_2\mathcal{L}_2+\lambda_3\mathcal{L}_3$
end
Output: Optimized parameters θ

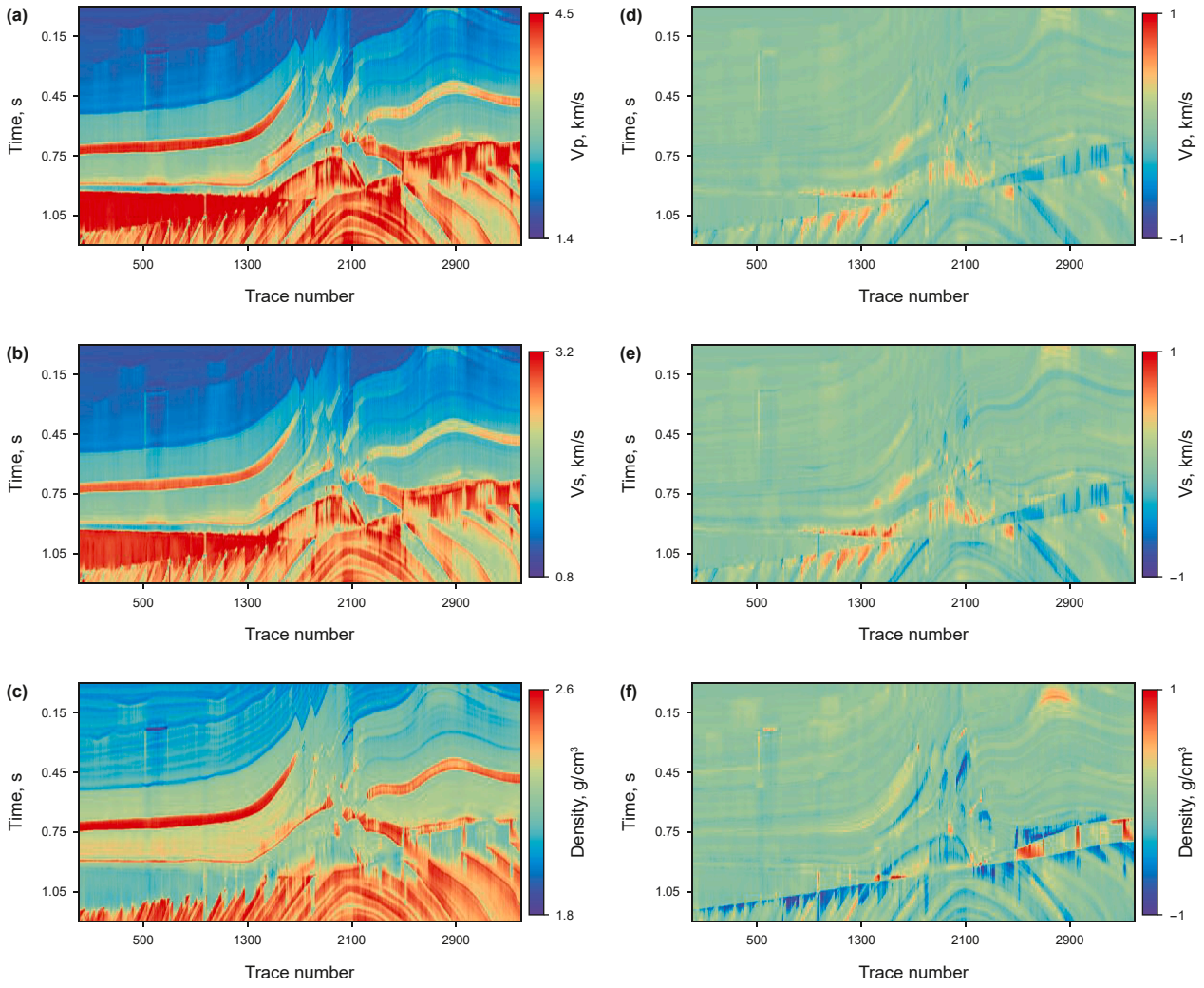

Fig. 5. The inversion results achieved using MGNN: **(a)** Vp, **(b)** Vs, and **(c)** density. Normalized profile of the difference between the reference value and the inverted results of **(d)** Vp, **(e)** Vs, and **(f)** density.

2.4. Spatio-temporal neural network

Both the seismic records and the elastic parameters contain spatio-temporal changes due to depositional and propagation effects. In this paper, a spatio-temporal neural network (STNN) consisting of CNNs and RNNs is selected for forward and inversion modeling. The specific structure of the inversion network is displayed in Fig. 2. The inputs to the network are seismic data (i.e., near-, middle-, and far-angle gathers) and initial elastic parameter model including velocity and density, and the output of the network is the true elastic parameters. The forward network has the same structure as the inversion network, the difference being that the inputs to the forward network are elastic properties and the outputs are seismic records. In order to facilitate the reproduction of the numerical experiments, the specific parameters of the network are as follows. The input data is a tensor of size 600×6, including the angle gathers and the initial elastic parameters, where 600 is the data sampling length. The CNN block consists of two convolutional layers, each of which has 8 filters of size 5×1. The padding and dilation of each convolutional layer are set to 2 and 1, respectively. A dropout layer (dropout = 0.1) immediately follows the convolutional layer to prevent network overfitting. The ReLu function is adopted as the activation function after the first convolutional layer. The pooling layer can optionally be added after the convolutional layer, depending on the accuracy or speed demands of the network. In our experiments, we do not add pooling layers. Subsequently, the features extracted by the CNN block are fed into the RNN block. The RNN block contains a bidirectional gated recurrent unit (BiGRU) network, which introduces a bidirectional structure based on the GRU model to better capture the bidirectional dependencies of sequence data. The count of hidden features in the BiGRU layer is assumed to be 8. Finally, the results of the BiGRU layer are passed through the fully connected layer to obtain the final output. The output are elastic parameters of size 600×3. The learning rate and epoch are fixed at 0.01 and 1500, respectively, through a trial-and-error strategy. The network training is conducted using the Adaptive Moment Estimation (Adam) optimizer to update and optimize the model parameters. In this way, by substituting the designed STNN into the double-dual neural network framework, joint physics and

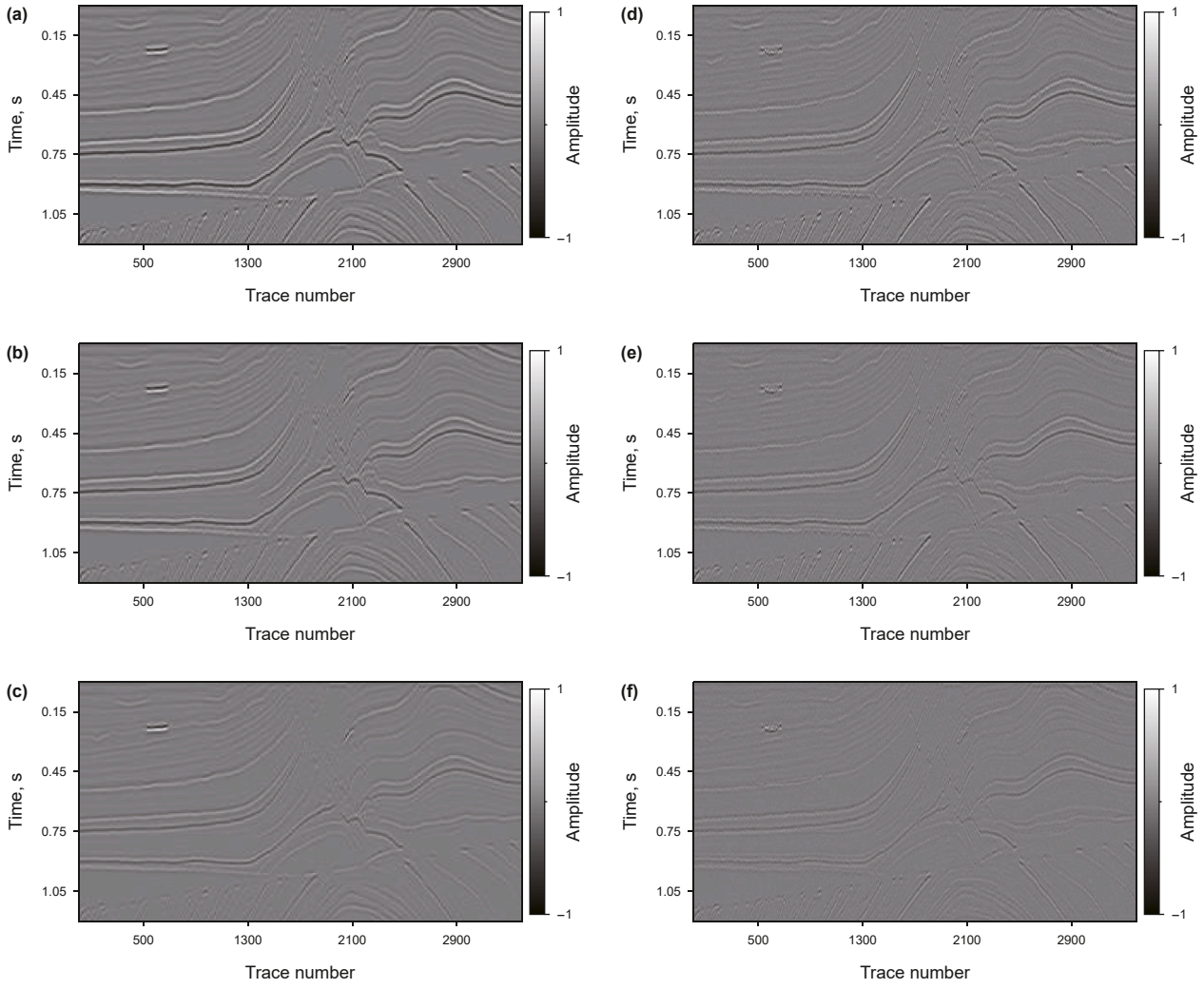

Fig. 6. **(a)** Near-, **(b)** middle-, **(c)** far-angle gathers reconstructed based on the inversion results of MGNN. **(d)**–**(f)** The difference profile between the reconstructed seismic records (Fig. 6(a)–(c)) and the reference seismic records (Fig. 4(d)–(f)).

model-guided deep learning-based seismic inversion can be implemented. In this experiment, we determine a relatively optimal set of network parameters based on experience and trial-and-error. However, this process is complex, and currently, there is no effective method to reliably determine the optimal network parameters. In subsequent experiments, to ensure a fair comparison, the same network structure is used for MGNN, PGNN and PMGNN. Moreover, for different tasks, various networks may achieve similar performance, and currently, there is no standardized approach or guideline. We use STNN as an illustration to check the feasibility of the proposed method, but other network frameworks (e.g., generative adversarial network, fully convolutional residual network, and fully-connected neural network et al.) can be incorporated into our proposed method.

3. Numerical examples

In this section, we demonstrate the effectiveness of the proposed method using simulated data from the benchmark Marmousi model and a field dataset. The numerical tests are performed using PyTorch as the backend on a personal computer with Windows 10, AMD Ryzen 7 5800X, and NVIDIA GeForce RTX 3080Ti. To show the applicability of the proposed method, we compare the results of the proposed method (i.e., PMGNN) with those of MGNN and PGNN. In addition, we adopt the root mean square error (RMSE) as shown below to quantitatively assess the goodness of the inversion results.

$$\mathrm{RMSE} = \sqrt{\frac{1}{N}\sum_{i=1}^{N}\left(m^i - \tilde{m}^i\right)^2} \tag{7}$$

where m and $\tilde{m}$ denote true values and inverted values, respectively. N stands for the sample size.

3.1. Synthetic example

By way of benchmark modeling, we use the Marmousi model (Fig. 3) as an example of inversion. The model contains 3400 traces with 600 time samples and a sampling interval of 2 ms. Fig. 3(a)–(f) display the reference models and initial models, respectively. The initial model here is obtained using a low-pass filtering technique based on the reference model, however, in general, it is possible to obtain it using commercial software based on known well data and seismic horizon. The corresponding noise-free near-, middle-, and far-angle gathers (Fig. 4(a)–(c)) are computed from the reference model (Fig. 3(a)–(c) using the Zoeppritz formula (Eq. (4)). In this case, a zero-phase Ricker wavelet with frequency of 30 Hz is adopted. To simulate real acquisition data, we add Gaussian white

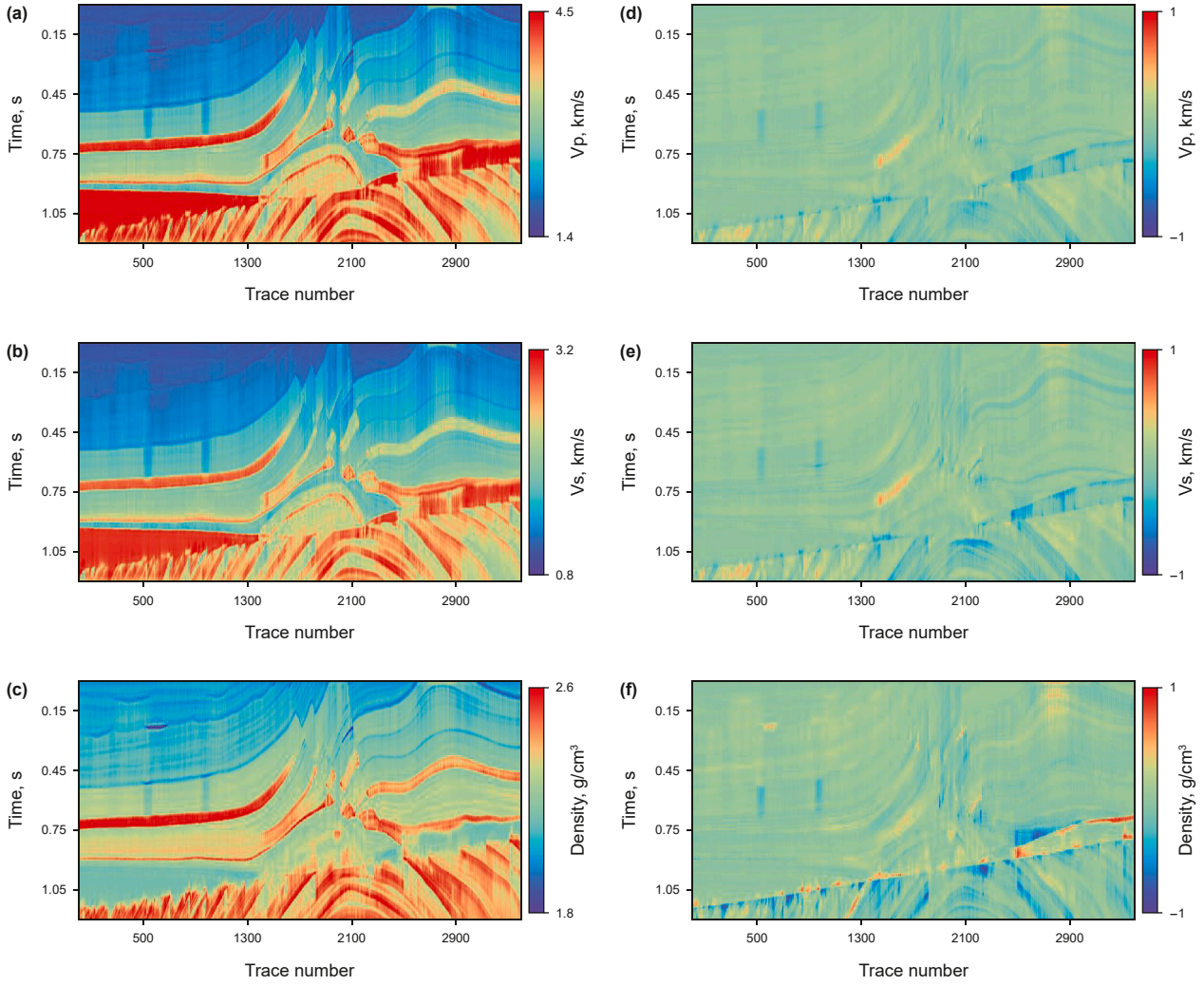

Fig. 7. The inversion results achieved using PGNN: **(a)** Vp, **(b)** Vs, and **(c)** density. Normalized profile of the difference between the reference value and the inverted results of **(d)** Vp, **(e)** Vs, and **(f)** density.

noise to the synthesized seismic data (Fig. 4(a)–(c)) to obtain noisy seismic data with a signal-to-noise ratio (SNR) of 5, as displayed in Fig. 4(d)–(f). The SNR is specified as $10\log_{10}\left(\|\mathbf{d}\|_2^2/\|\mathbf{d}-\tilde{\mathbf{d}}\|_2^2\right)$, where $\mathbf{d}$ and $\tilde{\mathbf{d}}$ stand for noise-free and noisy data, respectively. Noisy seismic data is utilized to invert elastic properties (i.e., P-wave velocity, S-wave velocity, and density). In this experiment, we randomly select 5 traces of data including seismic data and elastic properties to build training data pairs. In addition, we use the Zoeppritz equation (Eq. (4)) to construct the training dataset to train the forward neural network. By assuming that the forward network is known, the forward process is more easily compared to the inverse process, and the generalization ability of the trained forward neural network is good. During the training process, the forward neural network is utilized instead of the physical law, and the parameters of the forward network are kept fixed. Our goal is to construct a more robust inversion network to obtain reliable inversion results. The three methods (i.e., MGNN, PGNN and PMGNN) use the same inputs (i.e., seismic data and initial model) as well as labeled data. In addition, the structure of STNN used in the three methods is identical. The labeled and unlabeled data are subsequently fed into the three methods for inversion network training, which allows for prediction of elastic parameters. The training process for PMGNN and PGNN take approximately 180 s, with PGNN requiring slightly less computational time than PMGNN. In comparison, the training process for MGNN take around 120 s.

Fig. 5(a)–(c) display the inverted results of the P- and S-wave velocity and density using MGNN. The normalized difference profiles between the predicted Vp, Vs, and density of MGNN and the reference elastic parameters are illustrated in Fig. 5(d)–(f). The normalized difference profile is obtained by computing the difference between the inversion results and the true reference values, and then applying a normalization procedure. The inversion results of the MGNN generally reveal the subsurface strata, and the predictions are in good agreement with the reference model in gentle regions. However, in complex areas, a significant difference between the predictions and the reference model can be observed. In addition, since the MGNN is executed trace-by-trace, there are some vertical stripes in the inversion results, which could be interpreted as lateral discontinuities. The anomalous inversion results present in the inversion profiles of the MGNN prevent the stratigraphic boundaries from being clearly identified. To verify the correspondence between the inverted results and the observed seismic data, we compute synthetic seismic records of the inversion results, as shown in Fig. 6(a)–(c). Fig. 6(d)–(f) shows the

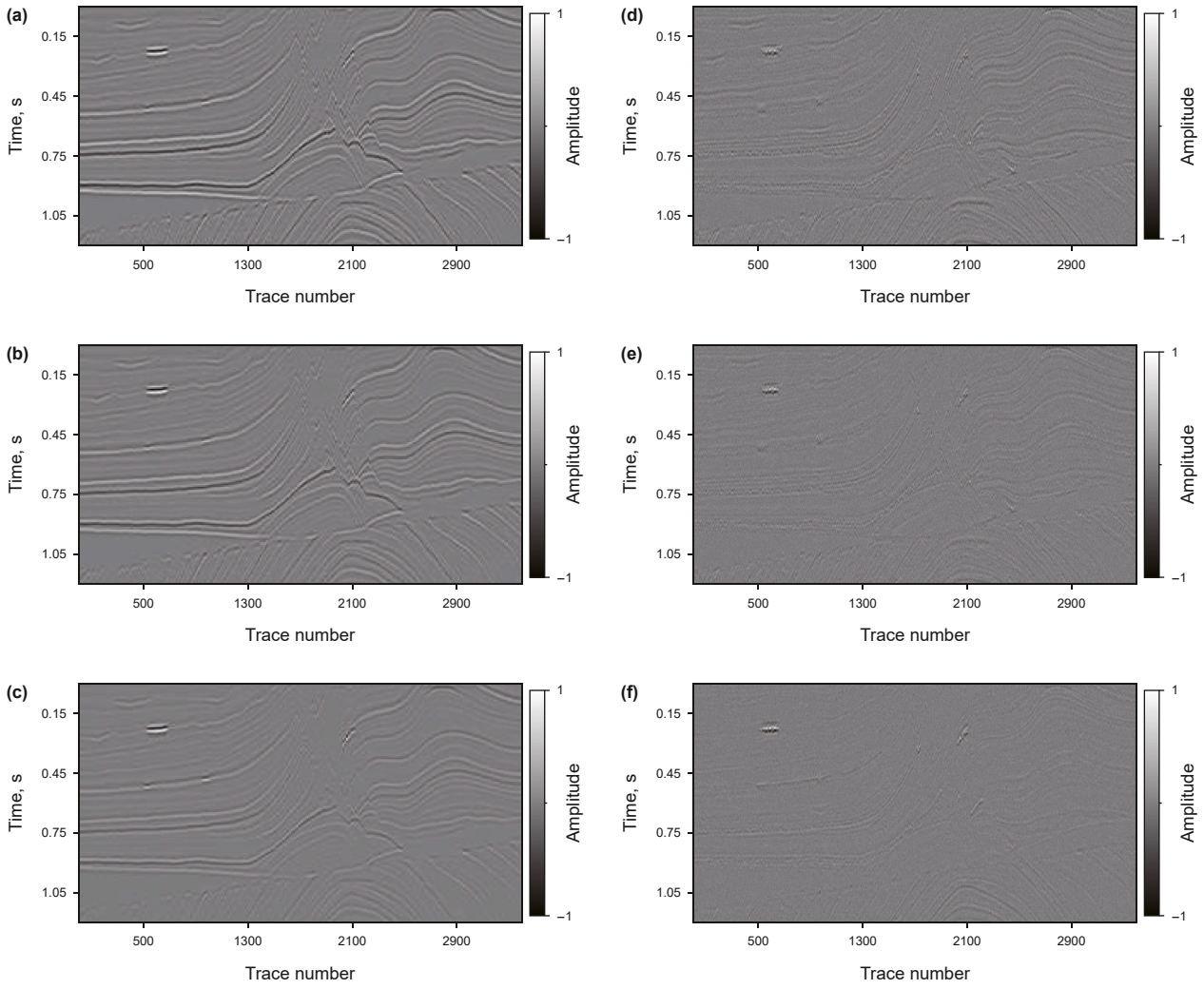

Fig. 8. **(a)** Near-, **(b)** middle-, **(c)** far-angle gathers reconstructed based on the inversion results of PGNN. **(d)**–**(f)** The difference profile between the reconstructed seismic records (Fig. 8(a)–(c)) and the reference seismic records (Fig. 4(d)–(f)).

difference profile between the seismic records (Fig. 6(a)–(c)) reconstructed based on the inversion results (Fig. 5(a)–(c)) and the reference seismic records (Fig. 4(d)–(f)). There are significant leaks of stratigraphic information in the differential profiles. MGNN considers only the contribution of labeled data to the network during the network training process and ignores the known laws of physics, resulting in prediction results that cannot be matched with observed seismic records. In other words, the limited training dataset does not guarantee that the trained network is applicable to the prediction of the whole profile, and the inverted results of MGNN do not satisfy the known laws of physics. Therefore, constraining the inversion results by introducing known physical laws should result in better results.

Fig. 7(a)–(c) illustrate the inverted results of the P-, S-wave velocity and density using PGNN. The normalized difference profiles between the inverted Vp, Vs, and density and the reference elastic parameters are displayed in Fig. 7(d)–(f). Compared to the inversion results of MGNN shown in Fig. 5, the lateral continuity in the PGNN inverted results profile is somewhat improved, and the anomalies are alleviated. The difference profiles intuitively show that the PGNN error is smaller compared to the MGNN error. Fig. 8(a)–(c) show the reconstructed seismic record based on the inversion results of the PGNN. Fig. 8(d)–(f) show the difference profile between the seismic records reconstructed (Fig. 8(a)–(c)) and the reference seismic records (Fig. 4(d)–(f)). Since PGNN considers known physical laws during network training, the reconstructed seismic records match well with the reference seismic records. PGNN integrates physical laws to make the prediction results satisfy the priori from the physical domain, which enhances the stability and accuracy of the inversion results. PMGNN further introduces priori information from the model domain, resulting in more stable inversion results and better recovery of stratigraphic detail information, as shown in Fig. 9(a)–(c). By comparing the difference profiles of the inversion results of the three methods, the errors of the inversion results of the three methods are small in the low-dip region. However, in the complex area, the error of the inverted results of PMGNN is smaller than those of MGNN and PGNN. PMGNN also considers known physical laws during the network training process, and the reconstructed seismic records based on its predictions match well with the reference seismic records, as illustrated in Fig. 10. The proposed method effectively enhances the accuracy of the prediction results and ensures the physical validity of the prediction results by introducing the information of physical laws and model domains through the double-dual network. As can be observed in Figs. 5, 7 and 9, vertical stripe artifacts are present in the inversion results.

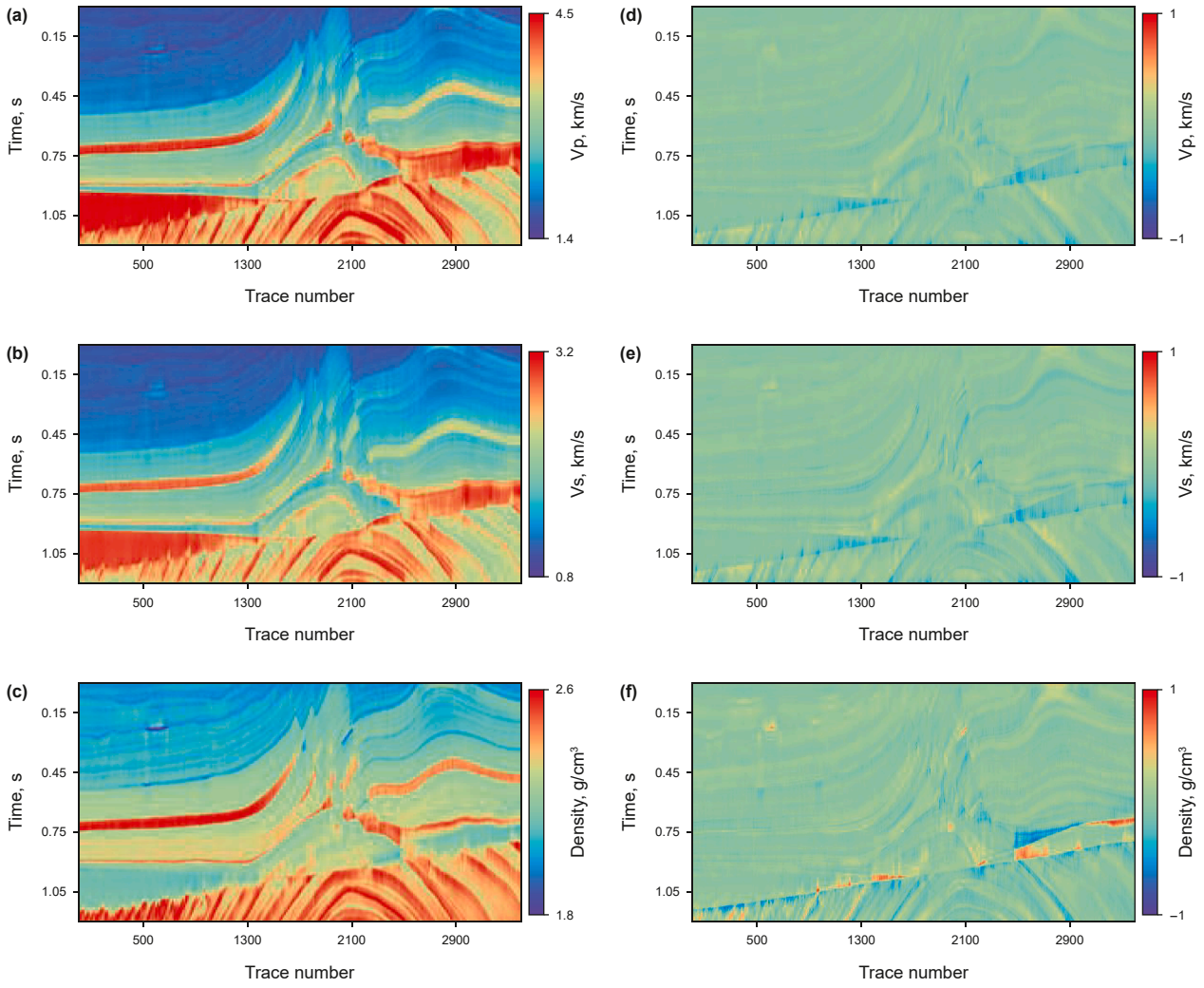

Fig. 9. The inversion results achieved using PMGNN: **(a)** Vp, **(b)** Vs, and **(c)** density. Normalized profile of the difference between the reference value and the inverted results of **(d)** Vp, **(e)** Vs, and **(f)** density.

Although the PMGNN method demonstrates certain improvements over MGNN, such artifacts remain evident. This issue may stem from the trace-by-trace inversion strategy adopted in this study, which neglects the spatial similarity between adjacent traces, thereby compromising lateral continuity. Additionally, given that the input seismic data are inherently noisy, the inversion results are susceptible to noise interference, leading to lateral discontinuities. The comparative analysis of the three inversion methods further illustrates that the proposed (PMGNN) method offers enhanced robustness to noise compared to the other approaches (MGNN and PGNN).

To quantitatively assess the advantages and disadvantages of the three methods, we calculate the normalized RMSE of each trace between their inversion results and the reference models. The normalized RMSE is computed by applying Eq. (7) to the normalized predicted results and reference values. Fig. 11 shows the histogram of normalized RMSE of MGNN, PGNN, and PMGNN. In agreement with the conclusions obtained from the previous inverted results, the MGNN method has the largest normalized RMSE due to the fact that it is a purely data-driven method and does not consider other priori information. PMGNN considers priori information from both the physical domain and the model domain, and its predicted results have the smallest error mean and a relatively narrow distribution. Fig. 12 illustrates the comparison of the normalized RMSE of the inversion results of MGNN, PGNN, and PMGNN for the whole profile and trace-by-trace. It is evident from the comprehensive inversion results that the PMGNN method achieves the smallest RMSE across the entire profile. In addition, as shown in Figs. 11 and 12, the normalized RMSE for velocity inversion results is similar, with the error in S-wave velocity being slightly higher than that of P-wave velocity. The largest error occurs in the density inversion results. This observation is consistent with the findings from model-driven inversion methods, indicating that density is less sensitive to the data compared to velocity. Furthermore, velocity and density curves at trace 2000 are illustrated in Fig. 13. There are obvious anomalies in the MGNN inversion results, which deviate from the reference values. PGNN introduces known physical laws, and its inversion results can better reflect the stratigraphic changes, but the low-frequency trends at some locations deviate from the reference. PMGNN considers both physical laws and model domain information, and its inversion results best match the reference values. Table 1 lists the normalized RMSE between the reference values and the predicted results of MGNN, PGNN, PMGNN at trace 2000. It

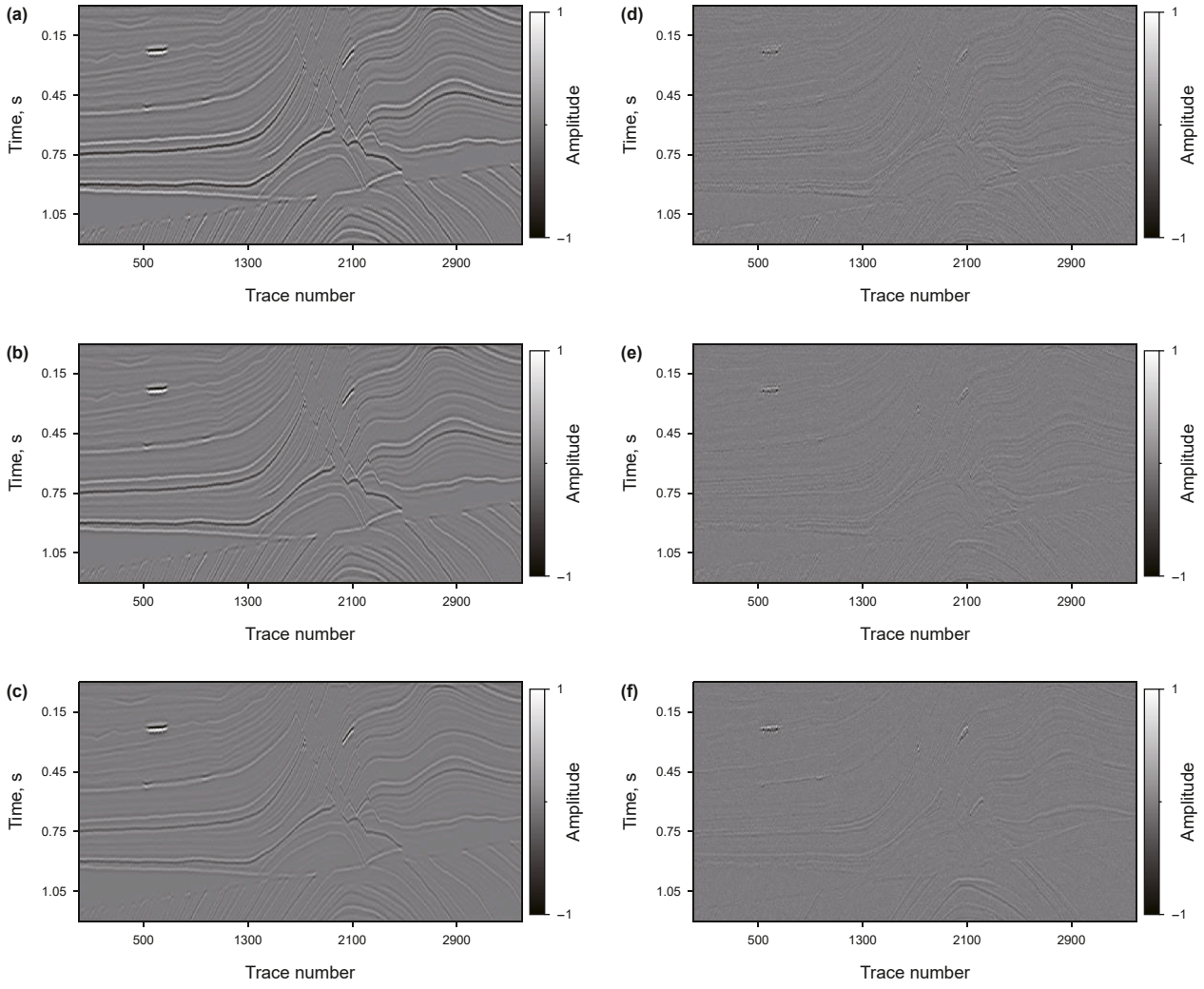

Fig. 10. **(a)** Near-, **(b)** middle-, **(c)** far-angle gathers reconstructed based on the inversion results of PMGNN. **(d)**–**(f)** The difference profile between the reconstructed seismic records (Fig. 10(a)–(c)) and the reference seismic records (Fig. 4(d)–(f)).

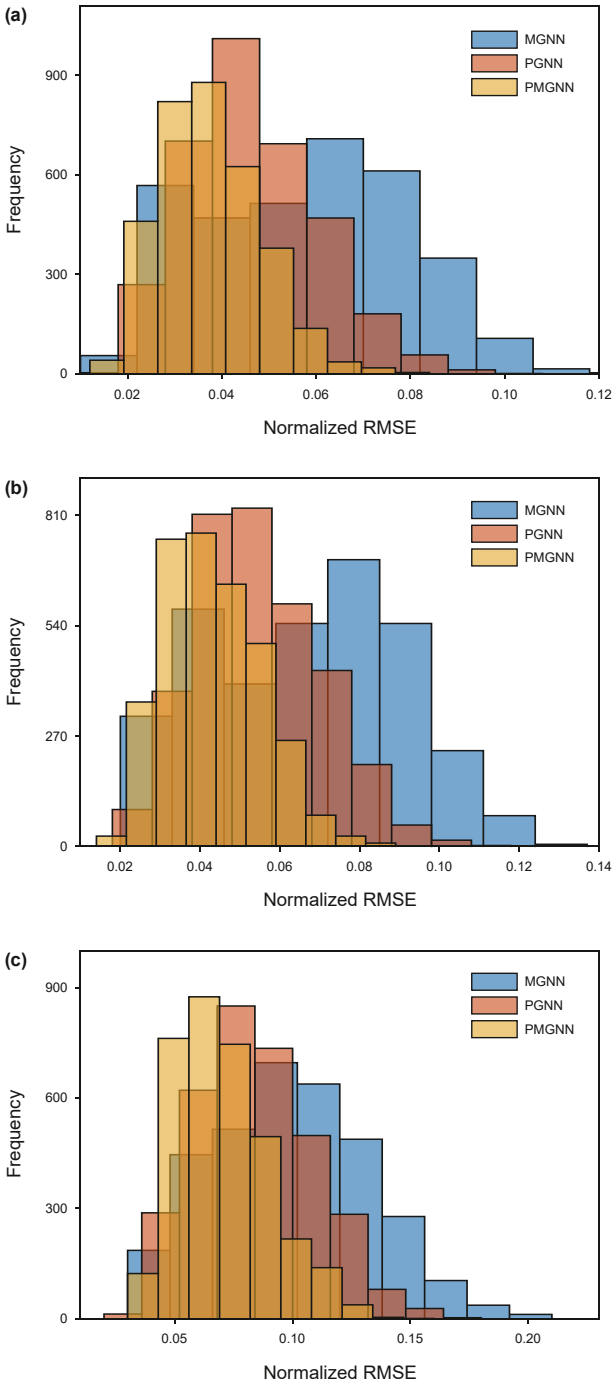

Fig. 11. Histogram of normalized root-mean-square error (RMSE) between MGNN, PGNN and PMGNN inversion results and reference values: **(a)** Vp, **(b)** Vs, and **(c)** density.

is evident that the PMGNN has the smallest normalized RMSE for Vp, Vs, and density. The qualitative and quantitative characterization of the prediction of the three methods in Figs. 5–13 and Table 1 illustrate that PMGNN has the optimal performance.

3.2. Field example

In light of the promising numerical results obtained in the synthetic tests, the utilization of 2D field data from north China allows us to further validate the efficacy and robustness of the proposed methodology. The crossing well profile used for the inversion test contains 110 traces and 311 samples with an interval of 2 ms, with two wells located at traces 41 and 84, respectively. Fig. 14(a)–(c) show the partially stacked angle gathers, termed near-, middle-, and far-angle gathers, where the blue lines mark the location of the well. The meticulous handling of measured seismic data has ensured the removal of noise and alignment of amplitude levels, thereby improving the overall quality and reliability of the data for further analysis. The low frequency (<10 Hz) initial Vp, Vs, and density established by specialized software based on the picked horizon and well logging curves are displayed in Fig. 15. Besides that, initial models can be obtained based on geological interpretation or seismic data processing. In the cross-well profile, one of the wells is used for training the network model. The training process followed the same procedure as that used for training with synthetic data. Prediction of elastic properties can be achieved by substituting seismic records and initial models into PMGNN.

Fig. 16 show the predicted results of the P-, S-wave velocity and density using MGNN. Well-log data is projected onto the inversion

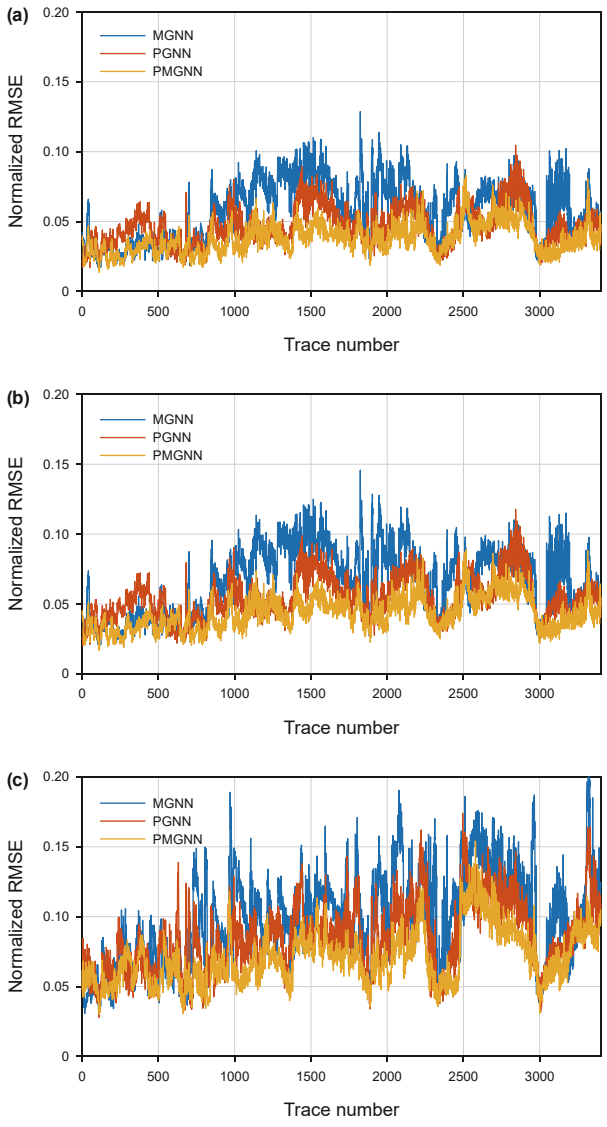

Fig. 12. Comparison of normalized RMSE on trace-by-trace for the inversion results of MGNN, PGNN, and PMGNN. **(a)** Vp, **(b)** Vs, and **(c)** density.

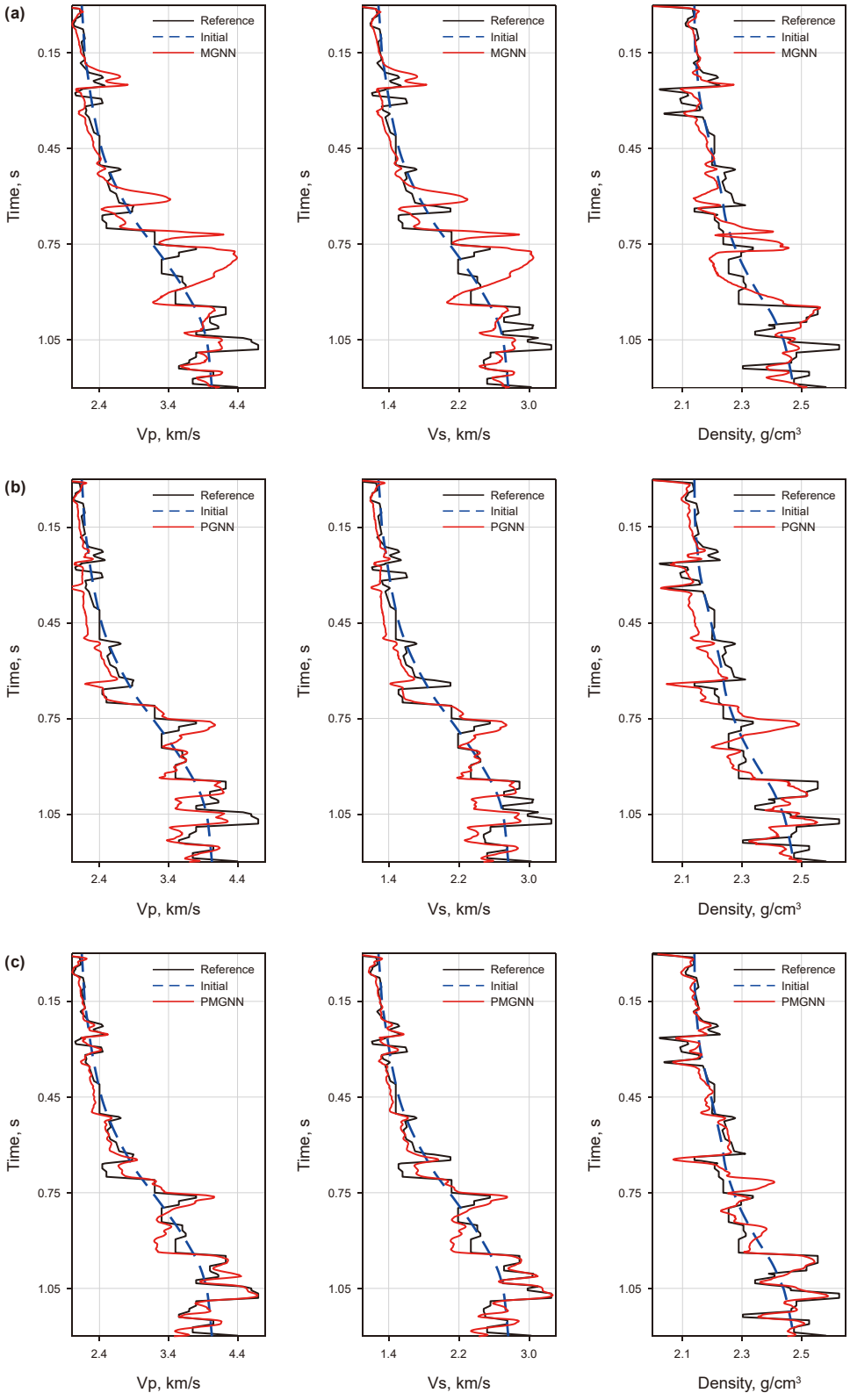

Fig. 13. Comparison of inverted elastic parameters of **(a)** MGNN, **(b)** PGNN and **(c)** PMGNN at trace 2000. The left panel shows the P-wave velocity, the middle panel shows the S-wave velocity, and the right panel shows the density. The black lines are the reference values, the blue dashed lines are the initial values, the red lines are the inversion results.

profile. In the experiment one well (at trace 41) is involved in the training of the network, while the other well (at trace 84) is served as a blind well for validating the effectiveness of the method. The predicted results of the MGNN generally reveal the subsurface strata with a significant improvement in resolution versus the initial model. Based on the inverted results, however, it is evident that certain anomalous values have reduced the lateral continuity of the profiles. The reconstructed seismic records based on the

Table 1
The normalized RMSE between the true and the inverted elastic parameters using MGNN, PGNN, and PMGNN for the Marmousi model at trace 2000.

	Vp	Vs	Density
MGNN	0.0684	0.0804	0.0925
PGNN	0.0453	0.0550	0.0847
PMGNN	0.0310	0.0333	0.0590

inversion results of the PGNN are shown in Fig. 17(a)–(c). Fig. 17(d)–(f) show the difference profile between the reconstructed seismic records (Fig. 17(a)–(c)) and the reference seismic records (Fig. 14). There is a significant error between the reconstructed seismic records based on inversion results and the reference seismic records because the MGNN method does not consider known physical laws.

Fig. 18(a)–(c) illustrate the predicted results of the P-, S-wave velocity and density using PGNN. Compared to the inverted results of MGNN, the horizontal continuity in the PGNN inverted results profile is somewhat improved, and the anomalies are alleviated. Fig. 19(a)–(c) show the reconstructed seismic record based on the inversion results of the PGNN. Fig. 19(d)–(f) show the difference profile between the seismic records reconstructed (Fig. 19(a)–(c)) and the reference seismic records (Fig. 14). Consistent with the conclusions obtained in the synthetic data

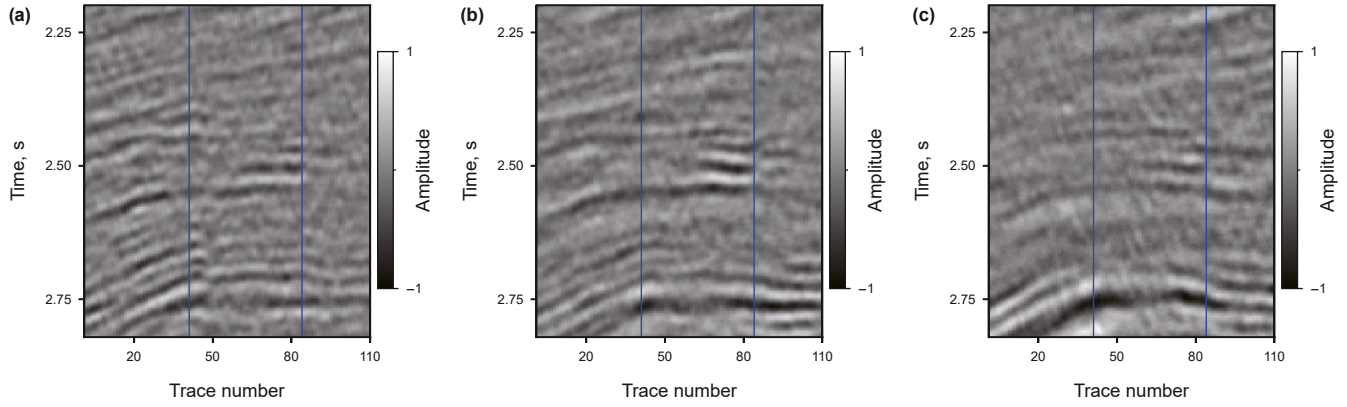

Fig. 14. Field case test: crossing-well sections of the partially stacked stacks. **(a)**–**(c)** near-, middle-, and far-angle gathers.

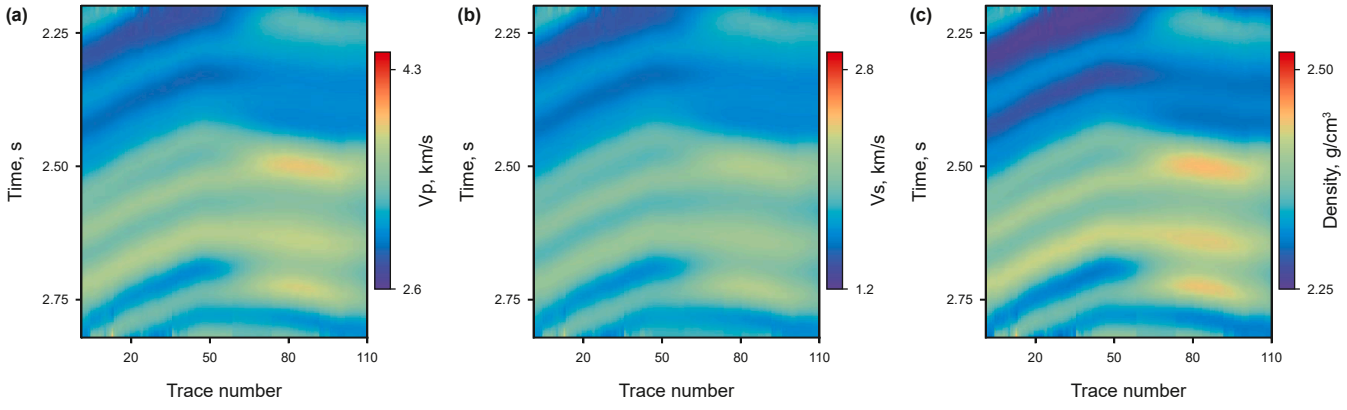

Fig. 15. The initial models of **(a)** Vp, **(b)** Vs, and **(c)** density.

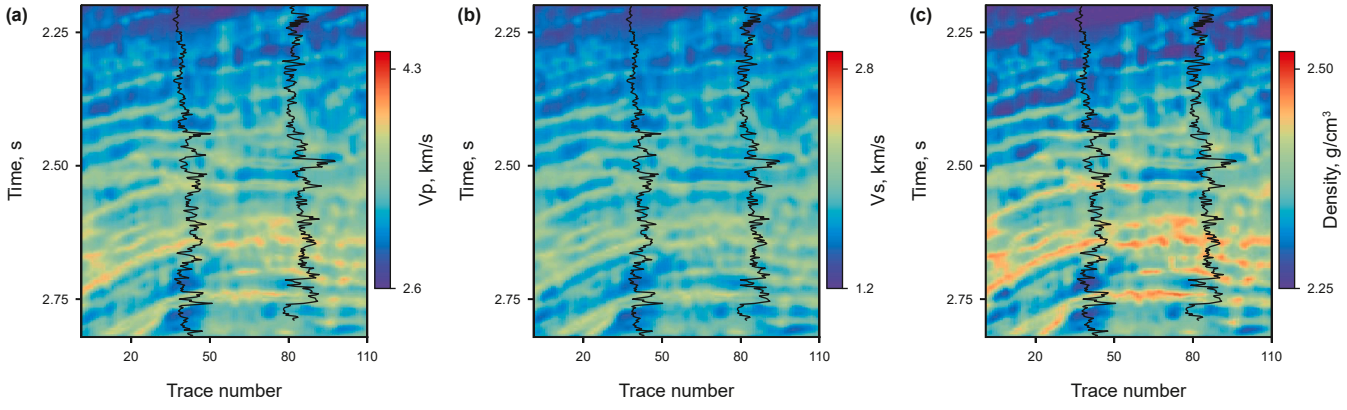

Fig. 16. The inversion results achieved using MGNN: **(a)** Vp, **(b)** Vs, and **(c)** density.

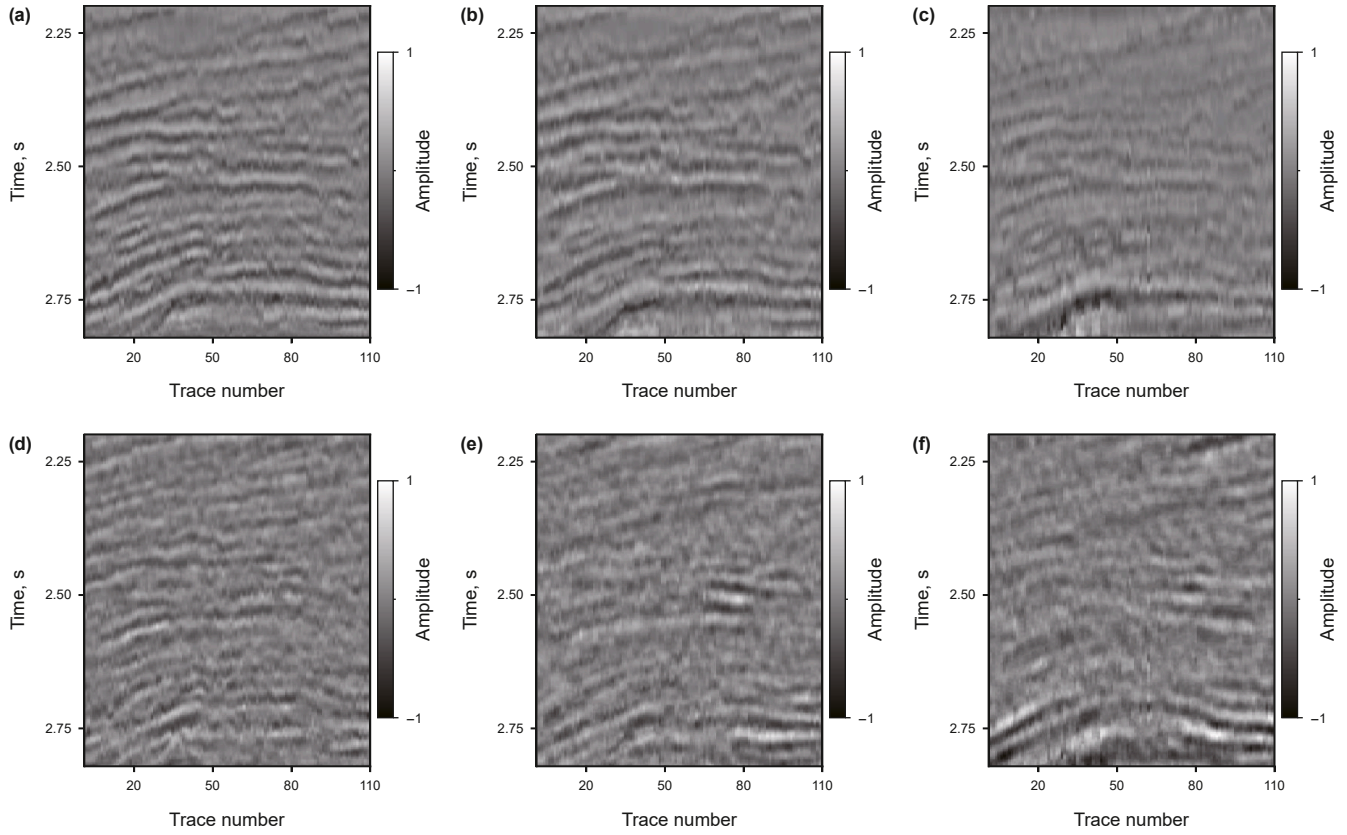

Fig. 17. **(a)** Near-, **(b)** middle-, **(c)** far-angle gathers reconstructed based on the inversion results of MGNN. **(d)**–**(f)** The difference section between the reconstructed seismic records (Fig. 16(a)–(c)) and the reference seismic records (Fig. 13(a)–(c)).

experiments, PGNN considers known physical laws during network training, and the reconstructed seismic records match well with the reference seismic records. PGNN integrates physical laws to make the prediction results satisfy the priori from the physical domain, which enhances the stabilization and accuracy of the inverted results. Fig. 20(a)–(c) illustrate the predicted results of the P-, S-wave velocity and density using PMGNN. The inversion results of PMGNN have the best lateral continuity, and the inversion results from this method are well matched with the well-log data. Fig. 21(a)–(c) show the reconstructed seismic record based on the inversion results of the PMGNN. Fig. 21(d)–(f) show the difference profile between the seismic records reconstructed (Fig. 21(a)–(c)) and the reference seismic records (Fig. 14). PMGNN also considers known physical laws during the network training process, and the reconstructed seismic records based on its predictions match well with the reference seismic records. The method considers both physical laws and model domain information, which enhances the accuracy and ensures the physical validity of the inversion results.

In order to investigate further the differences among the predicted results yielded by the MGNN, PGNN, and PMGNN, we focus our comparative analysis on a blind well located at trace 84, as

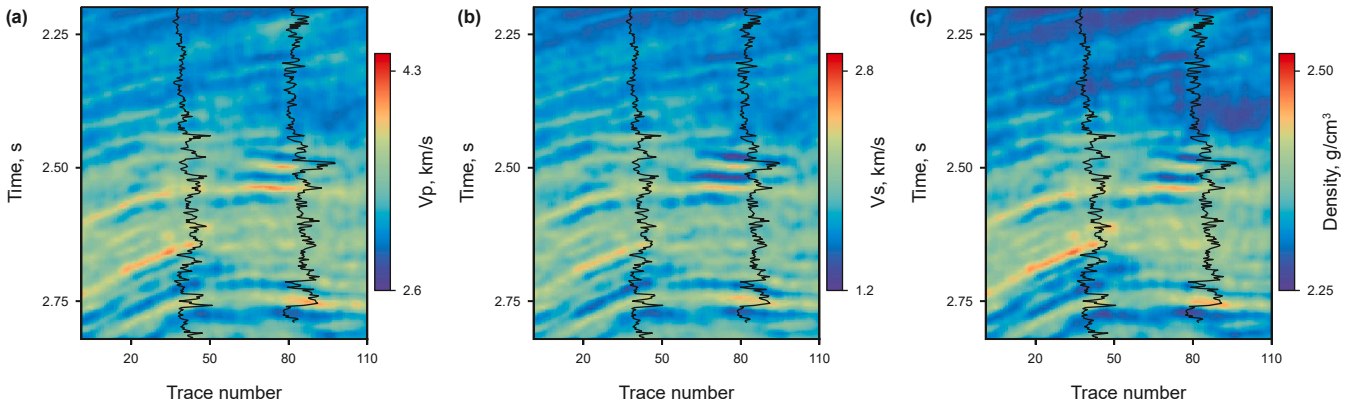

Fig. 18. The inversion results achieved using PGNN: **(a)** Vp, **(b)** Vs, and **(c)** density.

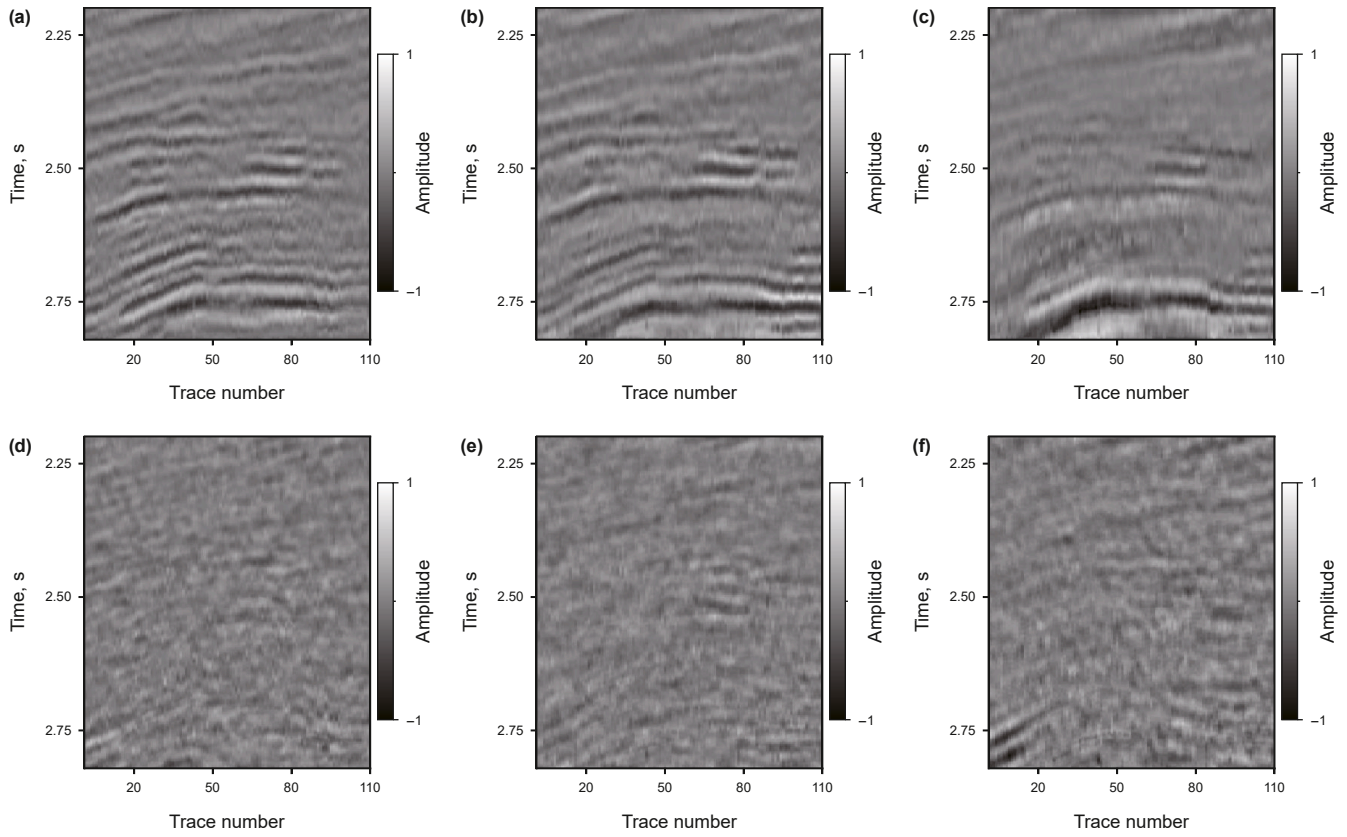

Fig. 19. **(a)** Near-, **(b)** middle-, **(c)** far-angle gathers reconstructed based on the inversion results of PGNN. **(d)**–**(f)** The difference section between the reconstructed seismic records (Fig. 18(a)–(c)) and the reference seismic records (Fig. 13(a)–(c)).

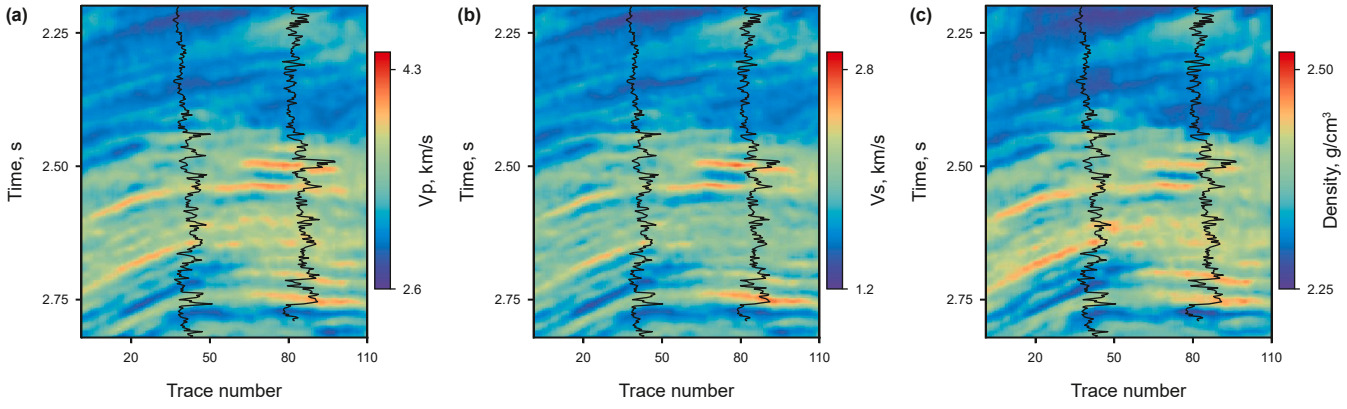

Fig. 20. The inversion results achieved using PMGNN: **(a)** Vp, **(b)** Vs, and **(c)** density.

shown in Fig. 22. The blind well data (black curves) are smoothed in advance to enable easier comparison. MGNN is limited by insufficient training data, and its inversion results at blind well locations have a low match with the reference curves. PGNN introduces known physical laws whose inversion results closely match the relative change of the reference curve. PMGNN further introduces the priori information of the model domain based on PGNN, and the inversion results obtained best match the reference curves. The normalized RMSEs of the three methods are listed in Table 2, which quantitatively illustrates the effectiveness of the proposed method. Meanwhile, it can be observed that the normalized RMSE of the density inversion results is greater than that of the velocity, which is consistent with the findings from the tests on synthetic data. In other words, density is less sensitive compared to velocity.

4. Discussion

Deep learning (DL) is a branch of artificial intelligence that has garnered significant attention and adoption across various industries due to its excellent performance and remarkable achievements. Specifically, within the discipline of seismic inversion, deep learning offers innovative approaches and methodologies that promise enhanced accuracy and efficiency. DL based seismic inversion methods are based on statistical theory, in which

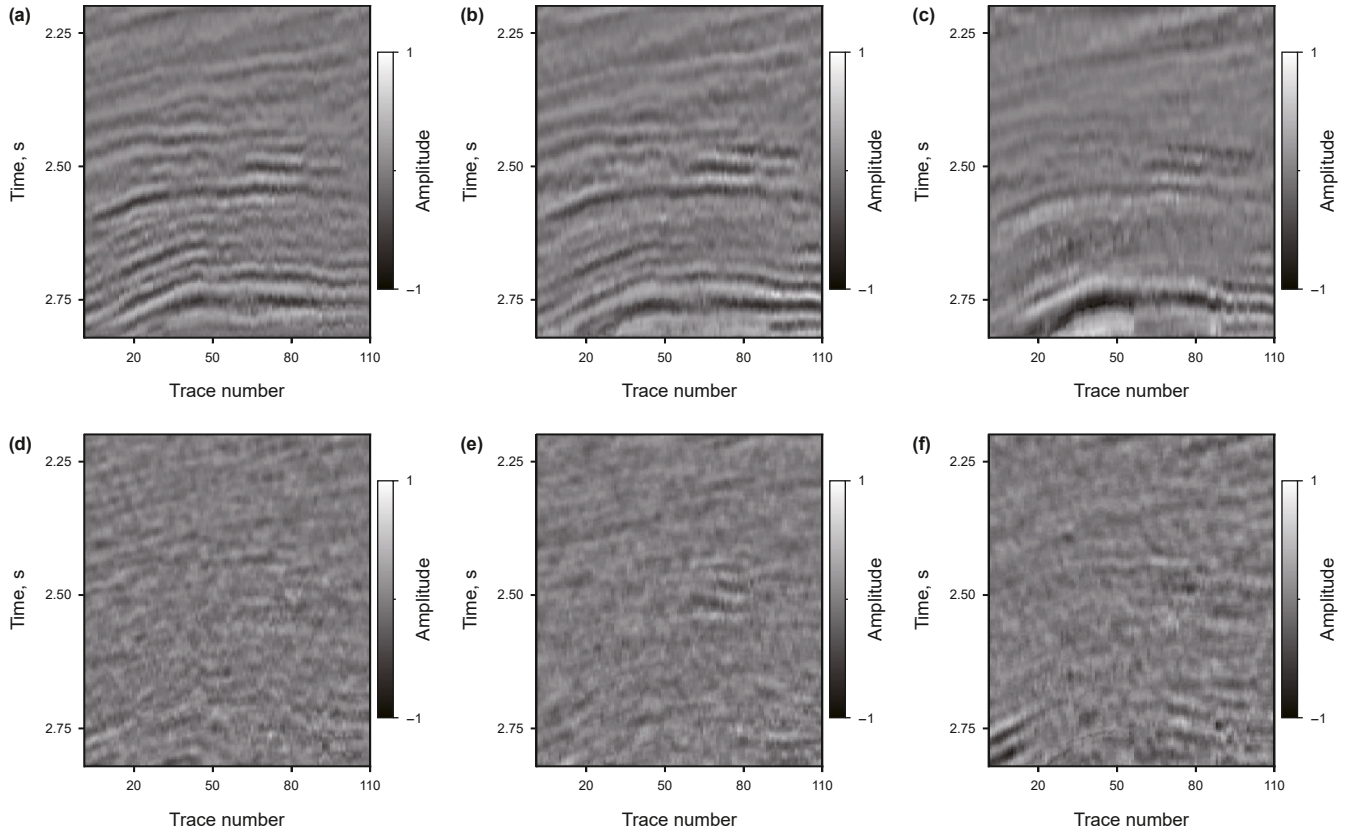

Fig. 21. **(a)** Near-, **(b)** middle-, **(c)** far-angle gathers reconstructed based on the inversion results of PMGNN. **(d)–(f)** The difference section between the reconstructed seismic records (Fig. 20(a)–(c)) and the reference seismic records (Fig. 13(a)–(c)).

a mapping between inputs and outputs can be learnt given enough training data pairs. The performance of deep learning depends on the type of network used and on the quality of the training data. The network training process makes physical sense only if the designed network architecture is aligned with the task to be trained. In this paper, considering the spatio-temporal characteristics of the elastic parameters and seismic data used in seismic inversion, a spatio-temporal neural network is used which helps to improve the effectiveness of network training. In different tasks, other network frameworks can be selected depending on the specific task requirements. Currently, there is no uniform standard for network selection, and the design of network parameters faces the same issue. In this paper, we set optimal network parameters using empirical and trial-and-error methods, as described in the main text.

The other key factor for the success of deep learning based seismic inversion is the training data. In real seismic surveys, it is difficult, if not impossible, to obtain high-quality and large-volume training datasets, which increases the difficulty of applying deep learning to seismic inversion. Due to the multi-solution nature of seismic inversion, physics-guided neural network (i.e., PGNN), which only considers physical laws, is unable to avoid the multi-solution challenge, although it can guarantee physical validity. In this paper, we develop a double dual neural network structure that joints both physics and model information (i.e., PMGNN) to alleviate the dependence of deep learning methods on training data. Introducing model domain information in additions to PGNN can greatly reduce non-uniqueness and give robust inversion results. The quality of the initial priori model can have a certain impact on the inversion results. In data-driven seismic inversion, if well data are available, the dependence on the initial priori model can be somewhat reduced. To evaluate the influence of the initial model quality on the inversion results of PMGNN, we conduct tests using the identical network architecture and training procedure with synthetic data, while only altering the initial models. New initial models are randomly generated from the true initial model during this process. The Structure Similarity Index Measure (SSIM) is employed to quantify the resemblance between the generated models and the true model, with larger SSIM values indicating closer agreement. As illustrated in Fig. 23, the normalized RMSE of the inversion results across the entire profile changes with varying SSIM values of the initial low-frequency model, reflecting the sensitivity of the proposed method to the quality of the initial model. It can be observed that as the initial model becomes closer to the true model, the normalized RMSE of the inversion results decreases. However, when the SSIM reaches 50%, the normalized RMSE begins to stabilize, indicating a reduced sensitivity of the inversion performance to further improvements in the initial model accuracy. Besides, stable 1D results have the same stable performance when spliced into 2D. However, the proposed method is still currently based on a trace-by-trace strategy for inversion, which cannot fully eliminate the lateral discontinuity. The presence of noise in the input seismic data is responsible for this phenomenon, as it can introduce lateral inconsistencies

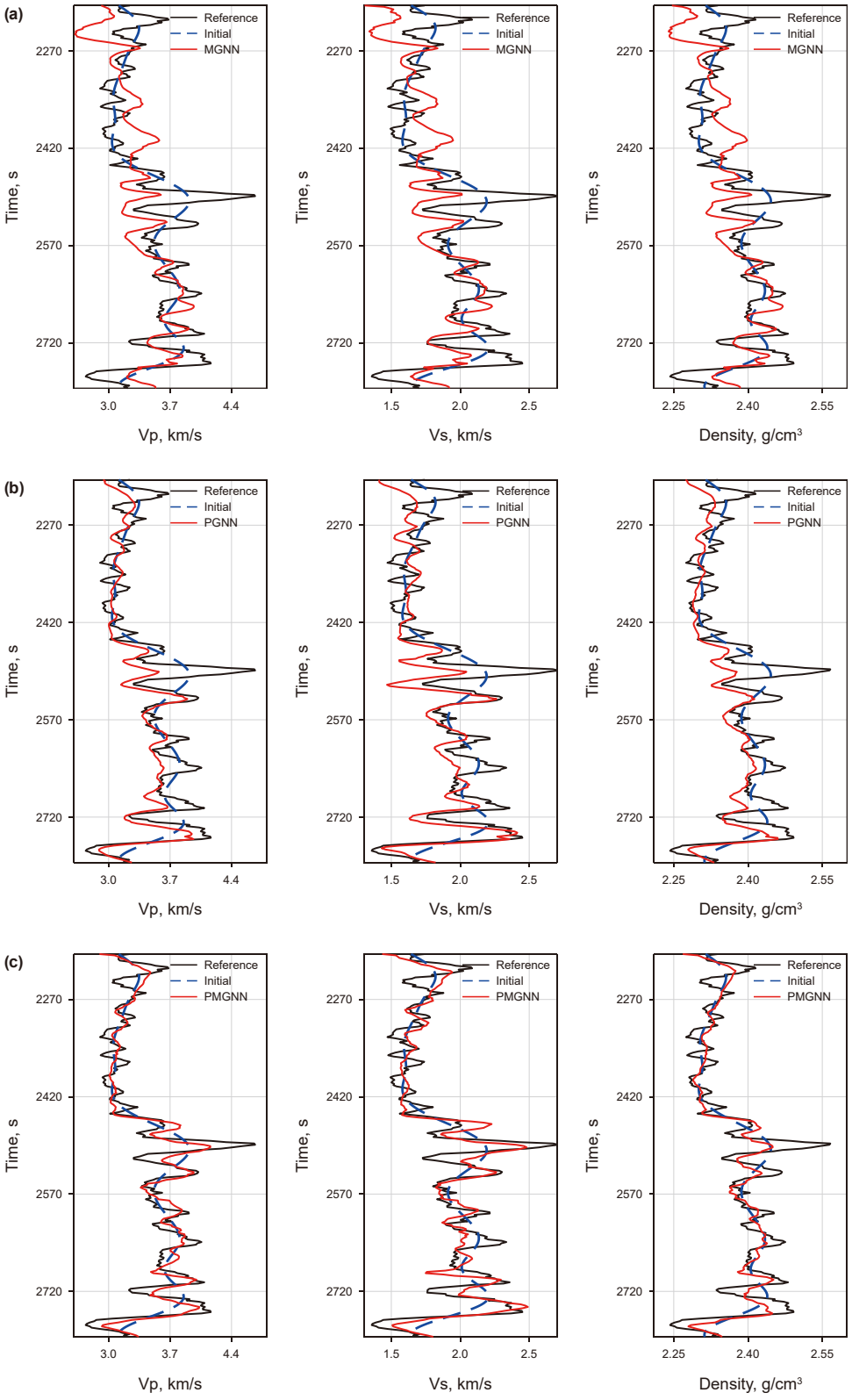

Fig. 22. Comparison of inverted elastic parameters of **(a)** MGNN, **(b)** PGNN and **(c)** PMGNN at trace 84. The left panel shows the P-wave velocity, the middle panel shows the S-wave velocity, and the right panel shows the density. The black lines are the reference values, the blue dashed lines are the initial values, the red lines are the inversion results.

Table 2
The normalized RMSE between the true and the predicted elastic properties using MGNN, PGNN, and PMGNN for field data at trace 84 (blind well).

	Vp	Vs	Density
MGNN	0.0946	0.1193	0.1330
PGNN	0.0780	0.1015	0.1144
PMGNN	0.0658	0.0869	0.0938

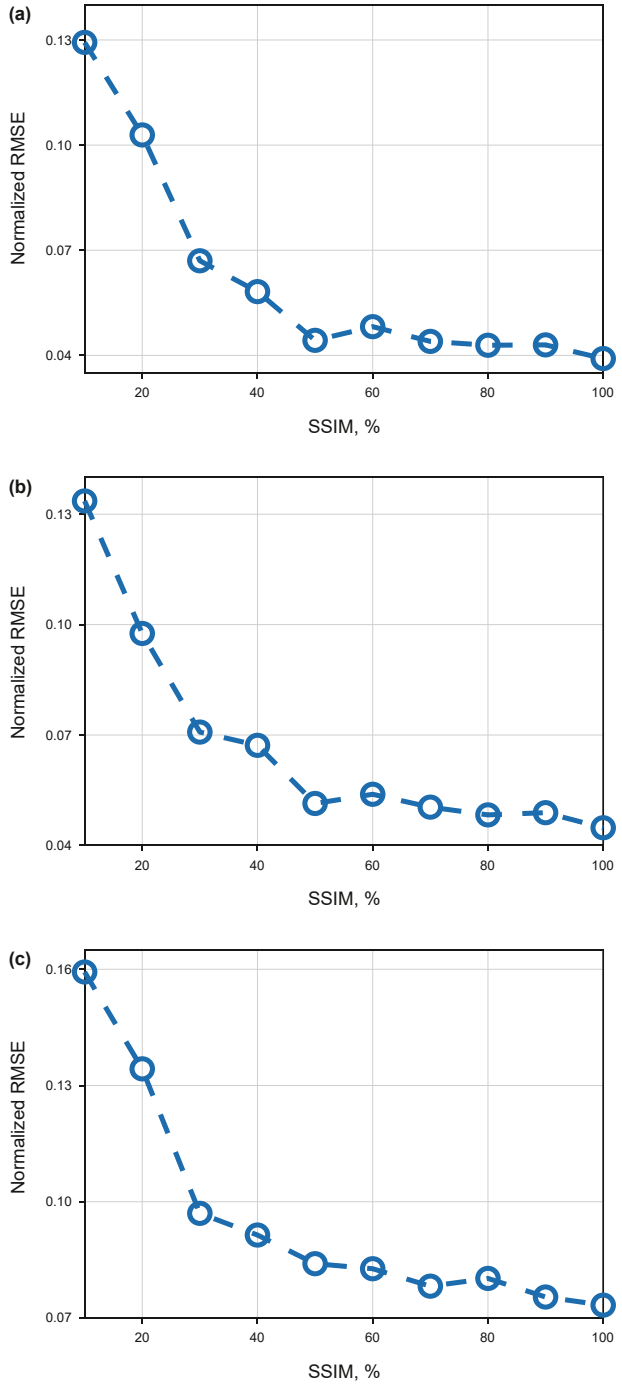

Fig. 23. The normalized RMSE of the inversion results varies with changes in SSIM. **(a)** Vp, **(b)** Vs, **(c)** density.

among adjacent traces in the inversion results. To further improve the lateral continuity of the inversion results, a multi-trace inversion strategy is a possible option for future work (Gholami, 2016; Veeken et al., 2009; Zhang et al., 2022a).

5. Conclusion

The inversion of seismic data to produce elastic parameter estimate is crucial in obtaining information for reservoir characterization. In this paper, we develop a double dual neural network structure that joints physics and model information to alleviate the dependence of deep learning based elastic parameter prediction methods on training datasets. The information from the different domains is linked through a loss function, where one dual network is responsible for constraining the inversion results using physics information to ensure the physical validity of the predictions, and the other dual network is responsible for constraining the inversion results using priori model information to improve the robustness of the predictions. The proposed method (PMGNN) has been evaluated on both synthetic datasets and field data, and its performance has been compared with that of MGNN and PGNN. PMGNN considers both physical laws and model domain information, and its inversion results best match the reference values. Both qualitative and quantitative assessments in synthetic and real data validate the advantages of PMGNN over MGNN and PGNN. Data-driven methods, as a promising approach for inverse problem solving, have the potential to achieve improved performance in seismic inversion by integrating more geophysically meaningful information. In this study, a loss function incorporating effective auxiliary information is proposed. Comparative analyses are carried out to assess the improvement in inversion performance achieved by integrating different types of information, offering valuable references for future efforts in information fusion within geophysical inversion frameworks.

CRediT authorship contribution statement

Jian Zhang: Writing – original draft, Methodology, Conceptualization. **Hui Sun:** Validation, Formal analysis. **Xing-Guo Huang:** Writing – review & editing, Methodology, Formal analysis, Data curation. **Li Han:** Writing – review & editing, Supervision. **Yan-Song Li:** Visualization.

Data availability

Model data and code associated with this research are available and can be obtained by contacting the corresponding author.

Declaration of competing interest

The authors declare that they have no known competing financial interests or personal relationships that could have appeared to influence the work reported in this paper.

Acknowledgements

This work was supported in part by the National Natural Science Foundation of China under Grant 42204108, 42374166 and 42374149, in part by National Key Laboratory of Petroleum Resources and Engineering, China University of Petroleum, Beijing under Grant PRE/open-2305, in part by Research on Fine Exploration and Surrounding Rock Classification Technology for Deep Buried Long Tunnels Driven by Horizontal Directional Drilling and Magnetotelluric Methods Based on Deep Learning under Grant E202408010.

References

Aleardi, M., Salusti, A., 2021. Elastic prestack seismic inversion through discrete cosine transform reparameterization and convolutional neural networks. Geophysics 86 (1), R129–R146. https://doi.org/10.1190/GEO2020-0313.1.

Alzahrani, H., Shragge, J., 2022. Seismic velocity model building using recurrent neural networks: A frequency-stepping approach. IEEE Trans. Geosci. Rem. Sens. 60, 1–9. https://doi.org/10.1109/TGRS.2022.3210899.

Arrowsmith, S.J., Trugman, D.T., MacCarthy, J., et al., 2022. Big data seismology. Rev. Geophys. 60 (2), e2021RG000769. https://doi.org/10.1029/2021RG000769.

Baddari, K., Aïfa, T., Djarfour, N., et al., 2009. Application of a radial basis function artificial neural network to seismic data inversion. Comput. Geosci. 35 (12), 2338–2344. https://doi.org/10.1016/j.cageo.2009.03.006.

Baddari, K., Djarfour, N., Aïfa, T., et al., 2010. Acoustic impedance inversion by feedback artificial neural network. J. Petrol. Sci. Eng. 71 (3–4), 106–111. https://doi.org/10.1016/j.petrol.2009.09.012.

Biswas, R., Sen, M.K., Das, V., et al., 2019. Prestack and poststack inversion using a physics-guided convolutional neural network. Interpretation 3 (3), SE161–SE174. https://doi.org/10.1190/INT-2018-0236.1.

Bosch, M., Mukerji, T., Gonzalez, E.F., 2010. Seismic inversion for reservoir properties combining statistical rock physics and geostatistics: A review. Geophysics 75 (5), 75A165–175A176. https://doi.org/10.1190/1.3478209.

Buland, A., Omre, H., 2003. Bayesian linearized AVO inversion. Geophysics 68 (1), 185–198. https://doi.org/10.1190/1.1543206.

Chen, H., Wu, B., Sacchi, M.D., et al., 2024. Multidimensional petrophysical seismic inversion based on knowledge-driven semi-supervised deep learning. IEEE Trans. Geosci. Rem. Sens. 62, 1. https://doi.org/10.1109/TGRS.2024.3460184.

Chen, Z., Zhang, Y., Gu, L., et al., 2023. Dual aggregation transformer for image super-resolution. In: 2023 IEEE/CVF International Conference on Computer Vision (ICCV), Paris, France, pp. 12278–12287. https://doi.org/10.1109/ICCV51070.2023.01131.

Das, V., Pollack, A., Wollner, U., et al., 2019. Convolutional neural network for seismic impedance inversion. Geophysics 84 (6), R869–R880. https://doi.org/10.1190/GEO2018-0838.1.

Daw, A., Karpatne, A., Watkins, W.D., et al., 2022. Physics-Guided Neural Networks (PGNN): an Application in Lake Temperature Modeling. Knowledge Guided Machine Learning. Chapman and Hall/CRC, pp. 353–372. https://doi.org/10.48550/arXiv.1710.11431.

Fabien-Ouellet, G., Sarkar, R., 2020. Seismic velocity estimation: a deep recurrent neural-network approach. Geophysics 85 (1), U21–U29. https://doi.org/10.1190/GEO2018-0786.1.

Feng, R., Balling, N., Grana, D., 2020. Lithofacies classification of a geothermal reservoir in Denmark and its facies-dependent porosity estimation from seismic inversion. Geothermics 87, 101854. https://doi.org/10.1016/j.geothermics.2020.101854.

Gao, Z., Li, C., Zhang, B., et al., 2021. Building large-scale density model via a deep-learning-based data-driven method. Geophysics 86 (1), M1–M15. https://doi.org/10.1190/GEO2019-0332.1.

Gholami, A., 2016. A fast automatic multichannel blind seismic inversion for high-resolution impedance recovery. Geophysics 81 (5), V357–V364. https://doi.org/10.1190/GEO2015-0654.1.

Grana, D., Russell, B., Mukerji, T., 2022. Petrophysical inversion based on *f-s-r* amplitude-variation-with-offset linearization and canonical correlation analysis. Geophysics 87 (6), M247–M258. https://doi.org/10.1190/GEO2021-0747.1.

Guo, R., Zhang, J., Liu, D., et al., 2019. Application of bi-directional long short-term memory recurrent neural network for seismic impedance inversion. In: 81st EAGE Conference and Exhibition 2019, London, the United Kingdom. https://doi.org/10.3997/2214-4609.201901386.

Guo, Y., Chen, J., Wang, J., et al., 2020. Closed-loop matters: Dual regression networks for single image super-resolution. In: IEEE/CVF Conference on Computer Vision and Pattern Recognition, ELECTR NETWORK. https://doi.org/10.1109/CVPR42600.2020.00545.

Kazei, V., Ovcharenko, O., Plotnitskii, P., et al., 2021. Mapping full seismic waveforms to vertical velocity profiles by deep learning. Geophysics 86 (5), R711–R721. https://doi.org/10.1190/GEO2019-0473.1.

Li, P., Grana, D., Liu, M., 2024. Bayesian neural network and Bayesian physics-informed neural network via variational inference for seismic petrophysical inversion. Geophysics 89 (6), M185–M196. https://doi.org/10.1190/GEO2023-0737.1.

Lin, Y., Theiler, J., Wohlberg, B., 2023. Physics-guided data-driven seismic inversion: recent progress and future opportunities in full-waveform inversion. IEEE Signal Process. Mag. 40 (1), 115–133. https://doi.org/10.1109/MSP.2022.3217658.

Liu, J., Zhao, L., Xu, M., et al., 2023. Porosity prediction from prestack seismic data via deep learning: incorporating a low-frequency porosity model. J. Geophys. Eng. 20 (5), 1016–1029. https://doi.org/10.1093/jge/gxad063.

Mousavi, S.M., Beroza, G.C., 2022. Deep-learning seismology. Science 377 (6607), 725. https://doi.org/10.1126/science.ahm4470.

Pan, X., Li, X., Huang, L., et al., 2024. Estimation of fracture properties from azimuthal seismic data using convolution neural network. IEEE Geosci. Remote Sens. Lett. 21, 1–5. https://doi.org/10.1109/LGRS.2024.3387699.

Röth, G., Tarantola, A., 1994. Neural networks and inversion of seismic data: Journal of geophysical research. Solid Earth 99 (B4), 6753–6768. https://doi.org/10.1029/93JB01563.

Saikia, P., Baruah, R.D., Singh, S.K., et al., 2020. Artificial neural networks in the domain of reservoir characterization: A review from shallow to deep models. Comput. Geosci. 135, 104357. https://doi.org/10.1016/j.cageo.2019.104357.

Shi, S., Li, M., Wang, J., et al., 2024a. Seimic impedance inversion based on semi-supervised learning. Comput. Geosci. 182, 105497. https://doi.org/10.1016/j.cageo.2023.105497.

Shi, Y., Yu, B., Zhou, H., et al., 2024b. FMG_INV, a fast multi-Gaussian inversion method integrating well-log and seismic data. IEEE Trans. Geosci. Rem. Sens. 62, 4503112. https://doi.org/10.1109/TGRS.2024.3351207.

Sun, J., Yang, J., Li, Z., et al., 2023. Intelligent AVA inversion using a convolution neural network trained with pseudo-well datasets. Surv. Geophys. 44 (4), 1075–1105. https://doi.org/10.1007/s10712-022-09766-5.

Sun, Q.H., Zong, Z.Y., Li, X., 2024. Probabilistic seismic inversion based on physics-guided deep mixture density network. Pet. Sci. 21 (3), 1611–1631. https://doi.org/10.1016/j.petsci.2023.12.015.

Veeken, P.C., Priezzhev, I.I., Shmaryan, L.E., et al., 2009. Nonlinear multitrace genetic inversion applied on seismic data across the Shtokman field, offshore northern Russia. Geophysics 74 (6), WCD49–WCD59. https://doi.org/10.1190/1.3223314.

Wang, J., Cao, J., Zhao, S., et al., 2022a. S-wave velocity inversion and prediction using a deep hybrid neural network. Sci. China Earth Sci. 65 (4), 724–741. https://doi.org/10.1007/s11430-021-9870-8.

Wang, P., Cui, Y., Liu, J., 2022b. Fluid discrimination based on inclusion-based method for tight sandstone reservoirs. Surv. Geophys. 43 (5), 1469–1496. https://doi.org/10.1007/s10712-022-09712-5.

Wang, Y.Q., Wang, Q., Lu, W.K., et al., 2022c. Seismic impedance inversion based on cycle-consistent generative adversarial network. Pet. Sci. 19 (1), 147–161. https://doi.org/10.1016/j.petsci.2021.09.038.

Wang, Y.Q., Wang, Q., Lu, W.K., et al., 2021. Physics-constrained seismic impedance inversion based on deep learning. IEEE Geosci. Remote Sens. Lett. 19, 1–5. https://doi.org/10.1109/LGRS.2021.3072132.

Xu, Y., Li, J., Chen, X., 2019. Physics informed neural networks for velocity inversion. In: Society of Exploration Geophysicists International Exposition and Annual Meeting 2019, San Antonio, TX, United states. https://doi.org/10.1190/segam2019-3216823.1.

Yu, B., Shi, Y., Zhou, H., et al., 2024. Fast Bayesian linearized inversion with an efficient dimension reduction strategy. IEEE Trans. Geosci. Rem. Sens. 62, 1. https://doi.org/10.1109/TGRS.2024.3360031.

Yu, S., Ma, J., 2021. Deep learning for geophysics: current and future trends. Rev. Geophys. 59 (3), e2021RG000742. https://doi.org/10.1029/2021RG000742.

Zhang, F., Zhu, L., Xu, X., 2024. A knowledge-embedded close-looped deep-learning framework for intelligent inversion of multisolution problems. Geophysics 89 (2), A17–A21. https://doi.org/10.1190/geo2023-0334.1.

Zhang, J., Zhao, X., Li, J., et al., 2022a. Structure-oriented prestack waveform inversion. Geophysics 87 (3), M73–M85. https://doi.org/10.1190/geo2021-0452.1.

Zhang, J., Zhao, X., Chen, Y., et al., 2023. Domain knowledge-guided data-driven prestack seismic inversion using deep learning. Geophysics 88 (2), M31–M47. https://doi.org/10.1190/geo2021-0560.1.

Zhang, J., Sun, H., Yuan, W., et al., 2022b. Post-stack impedance inversion based on spatio-temporal neural network. IEEE Geosci. Remote Sens. Lett. 19, 1–5. https://doi.org/10.1109/LGRS.2022.3227071.

Zhang, J., Li, J., Chen, X., et al., 2021. Robust deep learning seismic inversion with a priori initial model constraint. Geophys. J. Int. 225 (3), 2001–2019. https://doi.org/10.1093/gji/ggab074.

Zhou, L., Liu, X., Li, J., et al., 2021. Robust AVO inversion for the fluid factor and shear modulus. Geophysics 86 (4), R471–R483. https://doi.org/10.1190/geo2020-0234.1.

Zhu, S., Zhao, Z., Fang, P., et al., 2023. Improving scene text image super-resolution via dual prior modulation network. Proc. AAAI Conf. Artif. Intell. 37 (3), 3843–3851. https://doi.org/10.1609/aaai.v37i3.25497.

Zou, B., Wang, Y., Chen, T., et al., 2023. The domain adversarial and spatial fusion semi-supervised seismic impedance inversion. IEEE Trans. Geosci. Rem. Sens. 62, 1–15. https://doi.org/10.1109/TGRS.2023.3336392.